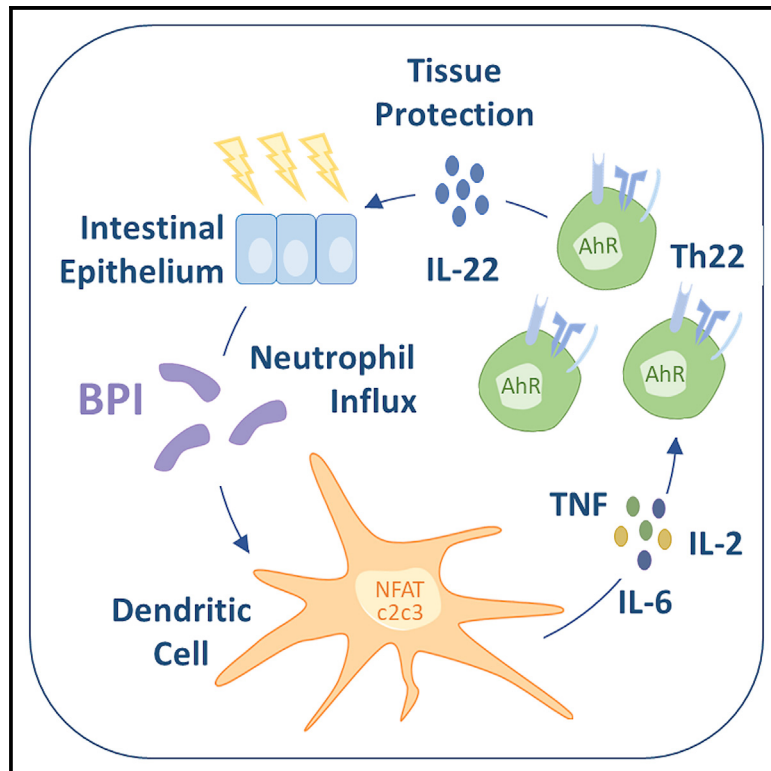


## Bactericidal/permeability-increasing protein instructs dendritic cells to elicit Th22 cell response

### Graphical abstract



### Authors

Sigrid Bülow, Katharina U. Ederer, Jonas M. Holzinger, ..., Andreas Hiergeist, Friederike Berberich-Siebelt, André Gessner

### Correspondence

sigrid.buelow@ukr.de

### In brief

Bülow et al. show that bactericidal/permeability-increasing protein (BPI) has substantial relevance in intestinal homeostasis. Following activation of murine dendritic cells by BPI, CD4<sup>+</sup> T cells predominantly differentiate into IL-22-secreting Th22 cells. This BPI-DC-IL-22 axis is fostered by diversification of intestinal microbiota and improves the outcome of dextran sodium sulfate-induced colitis.

### Highlights

- Bactericidal/permeability-increasing protein (BPI) is an activator of dendritic cells (DCs)
- BPI-dependent DC activation mediates differentiation of naive CD4<sup>+</sup> T cells into Th22 cells
- *Bpi*<sup>-/-</sup> mice exhibit reduced IL-22 induction and increased disease severity during colitis
- Microbiota diversification fosters BPI-dependent activation of IL-22-positive CD4<sup>+</sup> T cells



## Article

# Bactericidal/permeability-increasing protein instructs dendritic cells to elicit Th22 cell response

Sigrid Bülow,<sup>1,4,\*</sup> Katharina U. Ederer,<sup>1</sup> Jonas M. Holzinger,<sup>1</sup> Lisa Zeller,<sup>2</sup> Maren Werner,<sup>1</sup> Martina Toelge,<sup>1</sup> Christina Pfab,<sup>2</sup> Sarah Hirsch,<sup>2</sup> Franziska Göpferich,<sup>1</sup> Andreas Hiergeist,<sup>1,2</sup> Friederike Berberich-Siebelt,<sup>3</sup> and André Gessner<sup>1,2</sup>

<sup>1</sup>Institute of Clinical Microbiology and Hygiene, University Hospital Regensburg, 93053 Regensburg, Germany

<sup>2</sup>Institute of Medical Microbiology and Hygiene Regensburg, University of Regensburg, 93053 Regensburg, Germany

<sup>3</sup>Institute of Pathology, University of Würzburg, 97080 Würzburg, Germany

<sup>4</sup>Lead contact

\*Correspondence: [sigrid.buelow@ukr.de](mailto:sigrid.buelow@ukr.de)

<https://doi.org/10.1016/j.celrep.2024.113929>

## SUMMARY

Neutrophil-derived bactericidal/permeability-increasing protein (BPI) is known for its bactericidal activity against gram-negative bacteria and neutralization of lipopolysaccharide. Here, we define BPI as a potent activator of murine dendritic cells (DCs). As shown in GM-CSF-cultured, bone-marrow-derived cells (BMDCs), BPI induces a distinct stimulation profile including IL-2, IL-6, and tumor necrosis factor expression. Conventional DCs also respond to BPI, while M-CSF-cultivated or peritoneal lavage macrophages do not. Subsequent to BPI stimulation of BMDCs, CD4<sup>+</sup> T cells predominantly secrete IL-22 and, when naive, preferentially differentiate into T helper 22 (Th22) cells. Congruent with the tissue-protective properties of IL-22 and along with impaired IL-22 induction, disease severity is significantly increased during dextran sodium sulfate-induced colitis in BPI-deficient mice. Importantly, physiological diversification of intestinal microbiota fosters BPI-dependent IL-22 induction in CD4<sup>+</sup> T cells derived from mesenteric lymph nodes. In conclusion, BPI is a potent activator of DCs and consecutive Th22 cell differentiation with substantial relevance in intestinal homeostasis.

## INTRODUCTION

Bactericidal/permeability-increasing protein (BPI) is a cationic antimicrobial protein extruded by neutrophil granulocytes either via degranulation<sup>1</sup> or formation of neutrophil extracellular traps<sup>2–4</sup>. BPI is known for its bactericidal activity against gram-negative bacteria as well as its anti-inflammatory capacities directed toward gram-negative lipopolysaccharide.<sup>4–6</sup> Despite this selectivity, BPI is elevated in infections of heterogeneous origin, including gram-positive bacteria,<sup>7</sup> fungi,<sup>8</sup> and viruses such as SARS-CoV-2.<sup>9,10</sup> Consistent with enhanced neutrophil activation,<sup>11–13</sup> increased *BPI* mRNA was additionally found in autoimmune disorders such as inflammatory bowel disease (IBD)<sup>14</sup> and is associated with vascular pathology in systemic lupus erythematosus<sup>15</sup> and psoriasis.<sup>13</sup> In general, the presence of activated neutrophils is closely linked to tissue destruction caused by the release of reactive oxygen species, proteolytic proteins, and other antimicrobial effectors.<sup>16</sup> Neutrophil-driven counter-regulatory processes to restore homeostasis are of major interest due to their potential therapeutic applications.<sup>16</sup> Lymphocyte-derived interleukin (IL)-22 is a key player in maintaining tissue integrity at barrier interfaces.<sup>17</sup> Its relevance in IBD and other diseases is underscored in many studies

including the success of exogenous IL-22 in clinical trials.<sup>17–20</sup> Although BPI lacked pro-inflammatory properties on its own, synergy with bacterial lipoproteins in human peripheral blood mononuclear cells was shown to induce IL-6 and tumor necrosis factor (TNF) secretion.<sup>7</sup> Interestingly, association of BPI with human monocyte-derived dendritic cells (DCs) was found upon encounter of blebs of gram-negative origin,<sup>21</sup> yet a potential pro-inflammatory property of BPI was not examined. Together, these data implicate an unexplored immune function of BPI via modulation of antigen-presenting cells.

## RESULTS

### BPI activates and matures BMDCs

GM-CSF-cultivated, murine bone-marrow-derived cells (BMDCs), containing both conventional dendritic cells (cDCs) and monocyte-derived macrophages,<sup>22</sup> were stimulated with BPI resulting in the secretion of cytokines (Figure 1A) with peak expression of *Il6*, *Il12b*, *Il23a*, and *Tnf* genes at 4 h (Figure 1B). Consistent with low IL-12 protein secretion, only minor *Il12a* gene expression was detectable (Figures 1A and 1B). Stimulation with BPI also led to an upregulation of co-stimulatory CD40, CD80, and CD86 compared to a



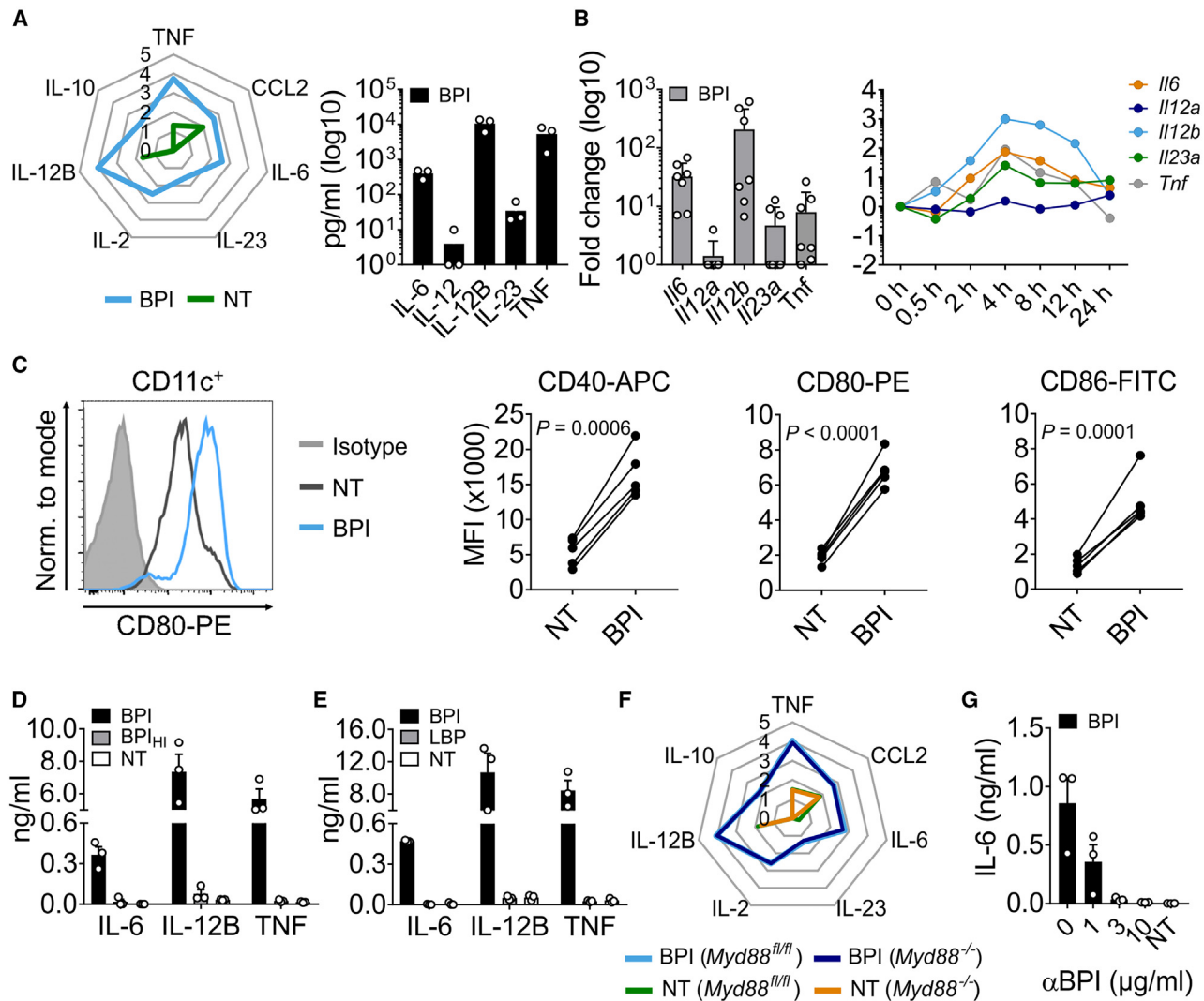


**Figure 1. BPI activates and matures BMDCs**

(A) Cytokine levels measured in the cell supernatant after BPI stimulation compared to untreated cells (NT;  $n = 3$ ). (B) Gene expression after BPI stimulation for 4 h ( $n = 7$ ) and in a kinetic approach. (C) Mean fluorescence intensity (MFI) of CD40, CD80, and CD86 after stimulation with BPI compared to untreated cells ( $n = 5$ ). (D and E) Cytokine secretion after stimulation with BPI and heat-inactivated BPI (BPI<sub>HI</sub>;  $n = 3$ , D) or LBP (E). (F) Cytokine secretion of BPI-stimulated *Myd88*<sup>fl/fl</sup> and *Myd88*<sup>-/-</sup> BMDCs ( $n = 3$ ). (G) BMDCs pre-incubated with indicated concentrations of a neutralizing  $\alpha$ BPI antibody and stimulated with BPI. Cytokine levels in spider diagrams are presented as pg/ml in a logarithmic scale (A and F). Results are shown as means  $\pm$  SEM (A, B, D, E, and G). Representative histograms and summarized data of flow cytometric analysis of CD11c<sup>+</sup> BMDCs are shown (C). Statistical testing was performed using Student's ratio paired t test. See also [Figure S1](#).

non-treated control (NT; [Figure 1C](#)). Heat-inactivated BPI (BPI<sub>HI</sub>) and the closely related lipopolysaccharide binding protein (LBP)<sup>22</sup> lacked immunostimulatory potency ([Figures 1D](#) and [1E](#); [Figures S1A](#) and [S1B](#)). Recombinant BPI purified with  $\alpha$ FLAG (BPI<sub>F</sub>) or ion exchange columns (BPI<sub>EX</sub>), as well as neutrophil-derived BPI (BPI<sub>N</sub>)-activated BMDCs comparably ([Figures S1C](#) and [S1D](#)). Both BPI<sub>F</sub> and BPI<sub>N</sub> associated with BMDCs ([Figure S1E](#)). Given the binding of toll-like receptor (TLR)2 and TLR4 ligands by BPI,<sup>4,7</sup> TLR dependency was excluded. BMDCs derived from C3H/HeJ mice defective in lipopolysaccharide (LPS) sensing by TLR4 remained BPI-

responsive ([Figure S1F](#)). BPI equally induced cytokines in *MyD88*<sup>fl/fl</sup> and *MyD88*<sup>fl/fl</sup>:CMV-cre (*MyD88*<sup>-/-</sup>) BMDCs ([Figures 1F](#) and [S1G](#)). Importantly, cytokine induction by BPI was specifically neutralized by an  $\alpha$ BPI antibody newly generated in mice ([Figure 1G](#)). In contrast to BMDCs, M-CSF-differentiated bone marrow-derived macrophages (BMDMs) and peritoneal lavage cells (PLCs) were not capable to respond with relevant cytokine secretion after stimulation with BPI ([Figures S1H](#) and [S1I](#)). Thus, we show that BPI preferably activates BMDCs in terms of a danger-associated molecular pattern (DAMP).

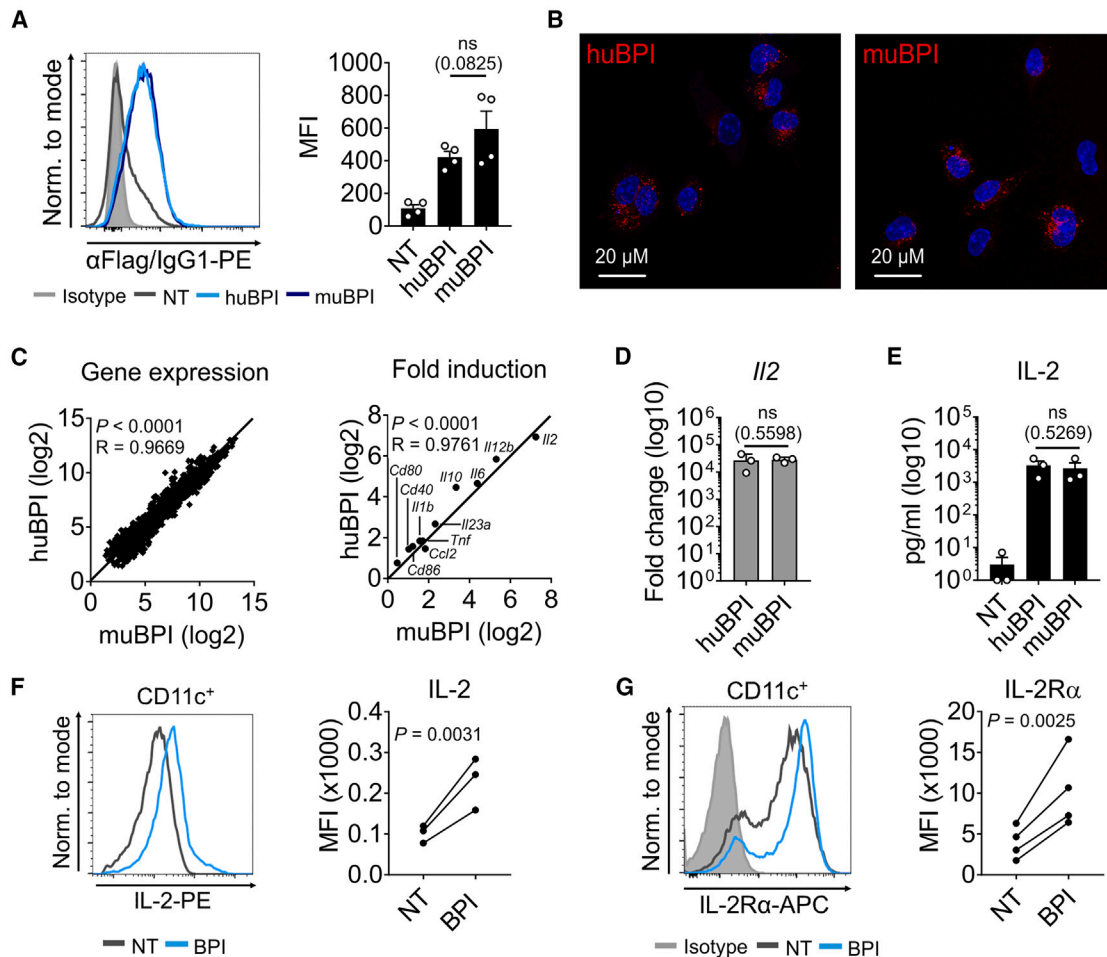


**Figure 2. BPI is a potent inducer of IL-2 in BMDCs**

(A) Cell association of BPI detected with an  $\alpha$ FLAG antibody after BMDCs were treated with FLAG-labeled huBPI and muBPI or left untreated ( $n = 4$ ). (B) Confocal microscopy of BMDCs incubated with human and murine Alexa 647-labeled BPI for 2 h (BPI: red, DAPI: blue). (C) Microarray analysis showing gene expression and fold induction of selected genes of BMDCs stimulated with huBPI and muBPI. Pearson's correlation was used for determination of the correlation coefficient  $R$ . (D and E) Analysis of IL-2 expression with RT-qPCR (4 h,  $n = 3$ ; D) and Luminex assays (18 h,  $n = 3$ ; E) after incubation with huBPI and muBPI. (F) IL-2 secretion by CD11c<sup>+</sup> BMDCs after BPI stimulation ( $n = 3$ ). (G) IL-2R $\alpha$  surface expression in CD11c<sup>+</sup> BMDCs upon BPI stimulation ( $n = 4$ ). Data are shown as means  $\pm$  SEM (A, D, and E). Representative histograms and the summarized data of flow cytometric analysis are shown (A, F, and G). Statistical testing was performed using Student's ratio paired  $t$  test. See also Figure S2.

### BPI induces IL-2 secretion in conventional DCs

For all experiments, human BPI (huBPI) was used unless indicated otherwise. Murine BPI (muBPI) displays a 53% amino acid identity to the human orthologue<sup>23</sup> and showed comparable association to BMDCs as seen by flow cytometry and confocal microscopy (Figures 2A and 2B). Of note, stimulation with both huBPI and muBPI revealed equivalent gene expression and protein levels for both orthologues as analyzed by GeneChip microarray, RT-qPCR, and Luminex assays, respectively (Figures 2C and S2A–S2C), thus indicating the absence of a species barrier. Expression of IL-2 was previously described in BMDCs.<sup>24</sup> However, the increase was, upon stimulation with BPI, surprisingly high. According to GeneChip microarray data of BMDCs, *Il2* was the most highly induced gene with a 152-

and 122-fold induction by huBPI and muBPI, respectively (Figure 2C). Equivalently high *Il2* gene and IL-2 protein expression was confirmed by RT-qPCR analysis, indicating a substantial 10<sup>4</sup>-fold increase, and by Luminex measurement, respectively (Figures 2D and 2E). IL-2 secretion assay revealed IL-2 production by the CD11c<sup>+</sup> population (Figure 2F). IL-2R $\alpha$  (also known as CD25) can be *trans*-presented to T cells by human monocyte-derived DCs and facilitates rapid T cell activation together with DC-derived IL-2.<sup>25</sup> Indeed, BPI also increased surface expression of IL-2R $\alpha$  on BMDCs (Figure 2G). Since BMDCs contain both macrophages and cDCs,<sup>22</sup> we also analyzed FLT3L- and GM-CSF-cultivated cDCs. Indeed, these cells also showed BPI-induced IL-2 production as well as BPI internalization comparable to BMDCs (Figures S2D–S2H). In

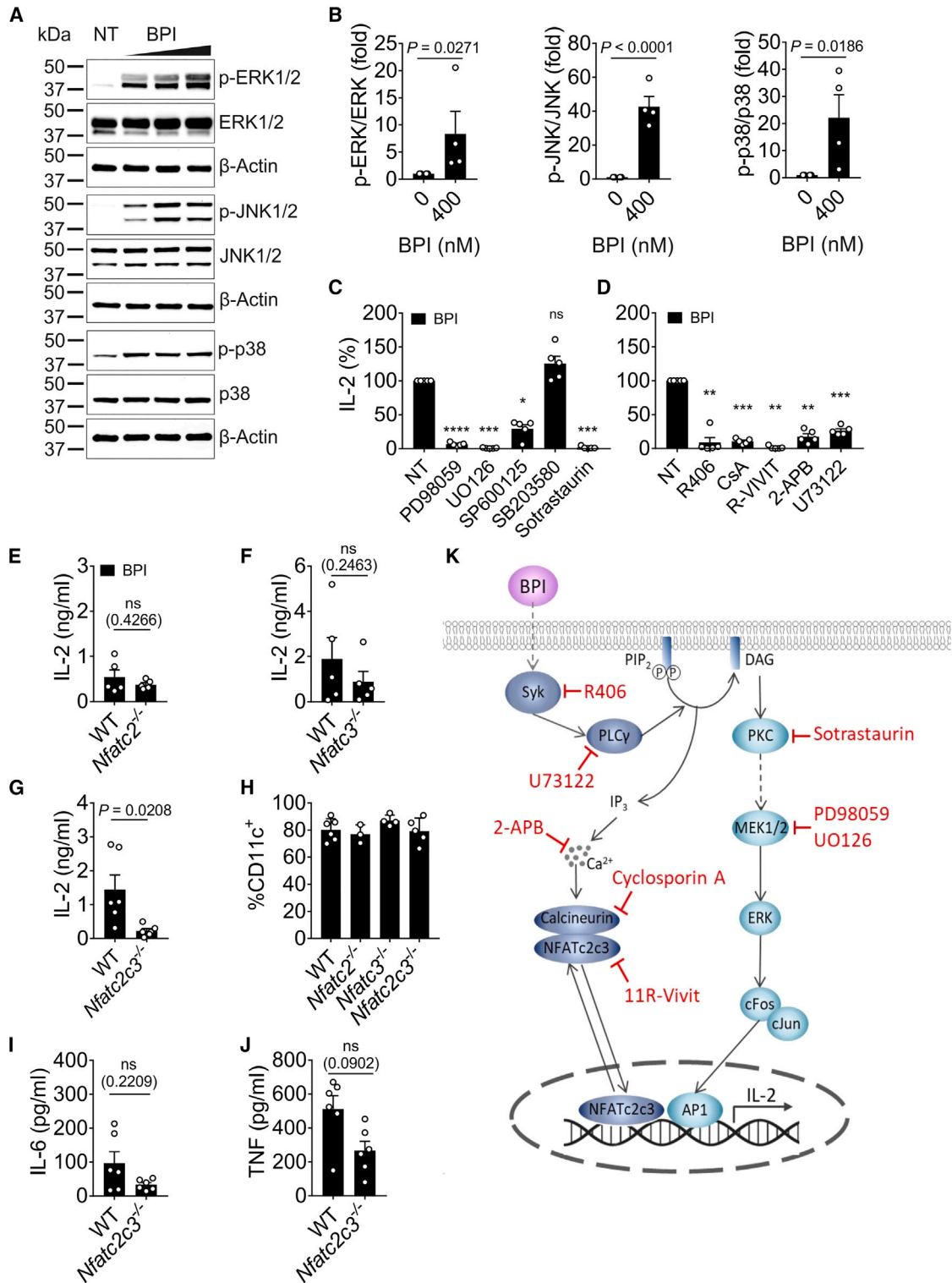


**Figure 3. BPI induces IL-2 in dependence of NFATc2c3**

(A) Western blot analysis of the phosphorylation status of ERK1/2, JNK1/2, and p38 kinases after stimulation with 100, 200, and 400 nM BPI (n = 3).

(B) Respective densitometric quantification of ERK, JNK, and p38 phosphorylation normalized to the corresponding unphosphorylated protein. Untreated controls were set as reference (n = 4).

(legend continued on next page)

contrast, M-CSF-differentiated and peritoneal macrophages did not secrete IL-2 upon BPI stimulation (Figures S2I). In conclusion, BPI has the potency to distinctly induce IL-2 secretion in BMDCs as well as FLT3L- and GM-CSF-cultivated cDCs as opposed to macrophages.

### BPI induces IL-2 in an NFATc2- and NFATc3-dependent manner

Concerning the underlying signaling pathway induced in BPI-stimulated BMDCs, phosphorylation of the mitogen-activated protein kinases ERK1/2, JNK1/2, and p38 was found (Figures 3A and 3B). Accordingly, inhibition of MEK1/2, the upstream kinases activating ERK1/2, by PD98059 and UO126 strongly reduced BPI-induced IL-2 production (Figure 3C). However, JNK inhibition by SP600125 showed a weaker effect and p38 inhibition by SB203580 had no effect (Figure 3C). Furthermore, PKC inhibition by sotrastaurin significantly inhibited BPI-induced IL-2 levels (Figure 3C). In accordance with its dependency on SYK in BMDCs,<sup>26</sup> BPI-induced IL-2 secretion was significantly inhibited by R406 (Figure 3D). Similar significant effects were obtained by specifically inhibiting PLC $\gamma$  with U73122, NFAT with 11R-VIVIT, by blocking calcineurin with cyclosporin A (CsA), and by reducing intracellular Ca<sup>2+</sup> availability through 2-APB (Figure 3D). Activation of NFATc2 by nuclear translocation in BMDCs was previously shown after stimulation with LPS.<sup>27</sup> Yet, BMDCs derived from *Nfatc2*<sup>-/-</sup> and also *Nfatc3*<sup>fl/fl</sup>:*Cd11c*-cre (*Nfatc3*<sup>-/-</sup>) mice showed no significantly reduced IL-2 levels after stimulation with BPI (Figures 3E and 3F). However, when using BMDCs from *Nfatc2*<sup>-/-</sup>:*Nfatc3*<sup>fl/fl</sup>:*Cd11c*-cre, i.e., double-deficient, mice (*Nfatc2c3*<sup>-/-</sup>), reduction of BPI-induced IL-2 secretion turned significant (Figure 3G). Of note, no differences in BMDC cell culture yield, proportion of CD11c<sup>+</sup> cells, and except for reduced upregulation of CD86 in *Nfatc2c3*<sup>-/-</sup> BMDCs, no significant difference in surface expression, namely CD40, and CD80, upon stimulation with BPI was observed for *Nfatc2*<sup>-/-</sup>, *Nfatc3*<sup>-/-</sup>, and *Nfatc2c3*<sup>-/-</sup> BMDCs (Figure 3H; Figures S3A–S3F). Expression of BPI-induced IL-6 and TNF also relied on ERK1/2, SYK, and intracellular Ca<sup>2+</sup>, albeit the decrease in NFATc2/c3-deficient cells did not reach significance (Figures 3I and 3J; Figures S3G–S3J). Thus, an NFATc2c3-dependent signaling pathway with concurrent contribution of the MAPKs ERK and JNK is proposed for BPI-induced IL-2 secretion (Figure 3K).

### BPI is an inducer of T cell activation *in vitro*

Since IL-2 mediates the activation of T cells, we stimulated lymphocytes with supernatants of BPI-stimulated (SN BPI) or non-treated (SN NT) BMDCs. Of note, all T cell experiments were performed without addition of external cytokines. Culturing of CD4<sup>+</sup> T cells with SN BPI in the presence of activating  $\alpha$ CD3 and  $\alpha$ CD28 antibodies resulted in cell clustering, a significant in-

crease in cell quantities on day (d)4 and d5, and secretion of IFN- $\gamma$ , IL-17A, and IL-22 (Figures 4A–4C). Importantly, induction of these cytokines disappeared when exchanging SN BPI for BPI (Figure S4A). In line with high levels of IL-6 and TNF in SN BPI, and their importance for IL-22 induction,<sup>28</sup> effects on IL-22 were more prominent than for IFN- $\gamma$  and IL-17A (Figure 4C). Flow cytometry revealed CD3<sup>+</sup>CD4<sup>+</sup> cells as producers of all three cytokines (Figures 4D and 4E; Figures S4B–S4G), whereby upregulated transcription factor AhR colocalized with IL-22-positive cells (Figures 4F and 4G). CD3<sup>+</sup>CD4<sup>+</sup> T cell activation was also shown by increase of IL-2R $\alpha$  and CD44 (Figures 4H and 4I). Application of SN BPI derived from *Nfatc2c3*<sup>-/-</sup> BMDCs markedly diminished IL-22 secretion without reducing IFN- $\gamma$  and IL-17A production (Figure 4J), and blockade of IL-2 with an IL-2-neutralizing antibody ( $\alpha$ IL-2) also only decreased IL-22 (Figure S4H). To summarize, BPI-stimulated BMDCs are capable of activating Th22 cells in an NFATc2/3-dependent manner.

### BPI fosters antigen-specific naive T cell differentiation *in vitro*

To evaluate whether BPI-mediated BMDC activation was strong enough to induce differentiation of T cells, IL-2R $\alpha$ <sup>+</sup>CD62L<sup>+</sup>CD44<sup>-</sup> sorted naive CD4<sup>+</sup> T cells of wild-type (WT) mice were incubated with SN BPI in the presence of  $\alpha$ CD3 and  $\alpha$ CD28, resulting in considerable T cell clustering, the release of IL-22, and only low levels of IL-17A (Figure 5A; Figure S4I). Congruent with the low level of IL-12 in SN BPI (Figures 1A and 1B), release of IFN- $\gamma$  was not detectable (Figure 5A). Antigen-specific T cell activation of CD4<sup>+</sup> T cells derived from OT-II transgenic mice confirmed upregulation of IL-2R $\alpha$  and CD44 as well as preferential release of IL-22 and low-level induction of IFN- $\gamma$  and IL-17A (Figures 5B–5E; Figure S4J). When naive CD4<sup>+</sup> T cells were used, distinct induction of IL-22 but not IFN- $\gamma$  or IL-17A occurred (Figure 5F). Therefore, stimulation of BMDCs with BPI mediates antigen-specific induction of Th22 cells from naive CD4<sup>+</sup> T cells.

### BPI promotes activation of T cells *in vivo*

Since both myeloid-derived IL-2 and lymphocyte-derived IL-22 are crucial for intestinal immune homeostasis and protection against chemical-induced colitis in mice,<sup>29,30</sup> we generated a BPI-deficient (*Bpi*<sup>-/-</sup>) mouse (Figures S5A–S5G) and investigated the role of BPI in the dextran sodium sulfate (DSS)-induced colitis model. Consistent with data in an independent BPI-deficient mouse model,<sup>31</sup> no significant weight loss was present after the acute phase. However, a significant difference was found in *Bpi*<sup>-/-</sup> compared to C57BL/6J WT mice during regeneration (d9–d12; Figure 6A). Accordingly, colon length in *Bpi*<sup>-/-</sup> mice was significantly shortened by d12 but not d7 (Figures 6B and 6C). However, on both d7 and d12, histology revealed a significantly higher, i.e., more severe disease score in *Bpi*<sup>-/-</sup> mice

(C and D) BPI-induced IL-2 secretion after incubation with indicated inhibitors compared to NT (n = 5).

(E–G) Secretion of IL-2 after BPI stimulation of *Nfatc2*<sup>-/-</sup> (E; n = 5), *Nfatc3*<sup>-/-</sup> (F; n = 5), and *Nfatc2c3*<sup>-/-</sup> (G; n = 6) BMDCs (BPI 100 nM).

(H) Summarized proportion of CD11c<sup>+</sup> BMDCs of WT (n = 6), *Nfatc2*<sup>-/-</sup> (n = 3), *Nfatc3*<sup>-/-</sup> (n = 4), and *Nfatc2c3*<sup>-/-</sup> (n = 5) as determined by flow cytometry.

(I and J) IL-6 (I) and TNF (J) concentrations for BPI-stimulated *Nfatc2c3*<sup>-/-</sup> BMDCs compared to corresponding WT cells (BPI 100 nM; n = 6).

(K) Schematic overview of the proposed pathways induced by BPI with inhibitors depicted in red. Data are shown as means  $\pm$  SEM (B–J) with \*p < 0.05, \*\*p < 0.01, \*\*\*p < 0.001, \*\*\*\*p < 0.0001. See also Figure S3.

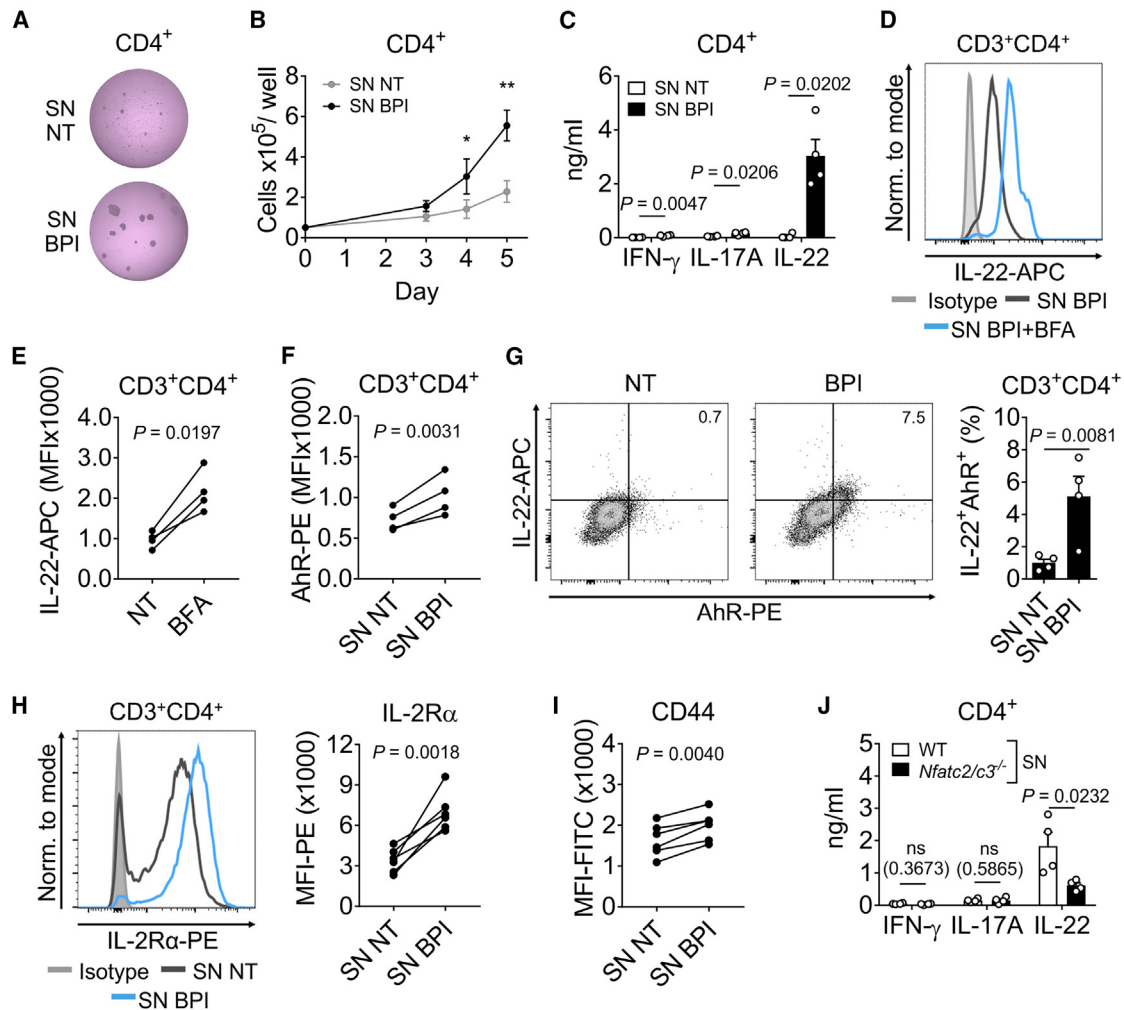


**Figure 4. BPI is an inducer of CD4<sup>+</sup> T cell activation**

(A and B) Representative light microscopic images (A) (d3, n = 4) and quantification of cell numbers (B) (d0, d3–d5) of CD4<sup>+</sup> T cells stimulated with SN BPI compared to SN NT (\*p = 0.048, \*\*p = 0.003; n = 6).

(C) Cytokine levels in the supernatants of CD4<sup>+</sup> cells stimulated with SN BPI for 24 h (CD4<sup>+</sup> pLNCs, 24 h, n = 4).

(D and E) Representative histogram (D) and MFI (E) for intracellular IL-22 in CD3<sup>+</sup>CD4<sup>+</sup> cells ± brefeldin A (BFA) stimulated with SN BPI (CD4<sup>+</sup> SCs, 72 h, n = 4).

(F) MFI for intracellular AhR in CD3<sup>+</sup>CD4<sup>+</sup> cells stimulated with SN BPI (CD4<sup>+</sup> SCs, 24 h, n = 4).

(G) Representative dot plot and percentages for IL-22<sup>+</sup>AhR<sup>+</sup>CD3<sup>+</sup>CD4<sup>+</sup> cells stimulated with SN BPI (CD4<sup>+</sup> spleen cells, 24 h, n = 4).

(H and I) Summarized MFIs for flow cytometric analysis of IL-2Rα (H) and CD44 (I) expression in CD3<sup>+</sup>CD4<sup>+</sup> cells activated by SN NT and SN BPI (pooled spleen cells and pLNCs, 16 h, n = 6). Representative histogram for IL-2Rα (H).

(J) Cytokine levels after stimulation with SN BPI derived from WT or *Nfatc2c3*<sup>-/-</sup> BMDCs (CD4<sup>+</sup> pLNCs, n = 4). Magnetic-activated cell sorting was performed in (A–G and J). Cells were activated in the presence of αCD3 and αCD28 antibodies (A–J). Images are in pseudocolor (A). Data are shown as means ± SEM (C, G, and J). Statistical testing was performed using Student's ratio paired t test. See also Figure S4.

with pronounced neutrophil influx (Figures 6D–6F; Figure S5H). Polyclonal restimulation of mesenteric lymph node (mLN) cells with αCD3 and αCD28 antibodies resulted in a significantly impaired cytokine response for IFN-γ (d7, d12), IL-22 (d7), and IL-2 (d12) for *Bpi*<sup>-/-</sup> mice (Figures S5I and S5J). A trend was seen for IL-17A and IL-2 levels on d7 (Figure S5I). No relevant response occurred without activating antibodies (Figure S5K). Differences *in vivo* could not be explained by immunophenotyping of untreated WT and *Bpi*<sup>-/-</sup> mice, which revealed equal lymphocyte composition in spleens, peripheral lymph nodes

(pLNs) and mLNs (Figures S6A–S6C), as well as comparable positivity for IL-22 in proximal and distal mLN cells (mLNCs; Figure S6D). IL-22 can impact the composition of intestinal microbiota by fostering expression of antimicrobial defense proteins. In order to abolish antimicrobial effects mediated directly by BPI or subsequently by IL-22, WT and *Bpi*<sup>-/-</sup> mice were co-housed 4 weeks prior to and during the course of acute DSS-induced colitis to allow continuous microbiota transfer. Despite an increased DSS dosage, differences in the cytokine pattern for IL-2, IFN-γ, IL-17, and IL-22 persisted in the

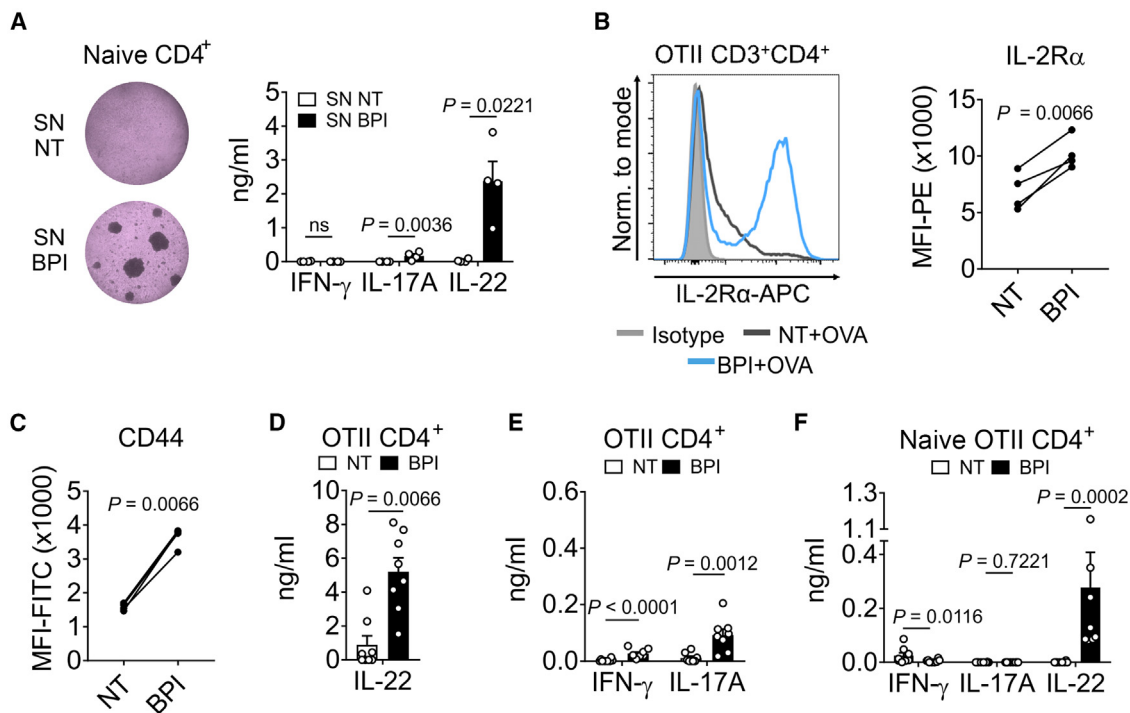


**Figure 5. BPI is an inducer of CD4<sup>+</sup> T cell activation and differentiation**

(A) Representative light microscopic images and cytokine levels in the supernatants of naive CD4<sup>+</sup> cells stimulated with SN NT or SN BPI (d5, n = 4). (B and C) IL-2R $\alpha$  (B) and CD44 (C) expression on CD4<sup>+</sup> OT-II T cells after 16 h of co-culture with OVA-loaded BMDCs previously stimulated with BPI for 18 h (n = 4). Representative histogram for IL-2R $\alpha$  in (B). (D) IL-22 levels in the supernatants of CD4<sup>+</sup> OT-II T cells after culture with OVA<sub>323-339</sub>-loaded BMDCs stimulated with 400 nM BPI (24 h, n = 8). (E) IFN- $\gamma$  and IL-17A levels in the supernatants of CD4<sup>+</sup> OT-II T cells after culture with OVA<sub>323-339</sub>-loaded BMDCs stimulated with 400 nM BPI for 24 h (n = 8). (F) Cytokine secretion by naive OT-II CD4<sup>+</sup> cells after culture with OVA<sub>323-339</sub>-loaded BMDCs stimulated with 400 nM BPI (5d, n = 8). Magnetic-activated (B–E) and additional fluorescence-activated cell sorting (A and F) was performed. Cells were activated in the presence of  $\alpha$ CD3 and  $\alpha$ CD28 antibodies (A). Images are in pseudocolor (A). Data are shown as means  $\pm$  SEM (A and D–F). Statistical testing was performed using Student's ratio paired t test. See also Figure S4.

restimulated mLNC (Figures 6G and 6H). No significant difference was detected for IL-4 and IL-10 (Figure 6I). The BPI-dependent increase in Th1, Th17, and Th22 cytokines during *ex vivo* restimulation indicates the potential of BPI to activate diverse T cell subsets. To determine the status *in vivo*, cytokines were measured in serum on d7 of colitis. Both IFN- $\gamma$  and IL-22 but not IL-17A were significantly decreased in *Bpi*<sup>-/-</sup> mice (Figure 6J). Remarkably, in accordance with *in vitro* data (Figures 4C and 4J, 5A, and 5D–5F), systemic IL-22 exceeded IFN- $\gamma$  levels on d7 (Figure 6J). To proof the potency of the BPI-DC-T cell axis to mediate intestinal protection, we transferred BMDCs either untreated or after 1 h of internalization of BPI. As published for BMDCs generated with GM-CSF and IL-4,<sup>33</sup> transfer caused significantly worse outcome in DSS-induced colitis as measured by weight, colon length, and histological score (d12; Figures S7A–S7C). Along with a pronounced upregulation of the Th22-specific transcription factor AhR (d7; Figure S7D), the difference was reversed in BMDCs pre-incubated with BPI (d12; Figures S7A–S7D). In summary, BPI significantly improves the outcome of DSS-induced colitis along with induction of T cell-derived IL-22 and upregulation of AhR, respectively. Moreover, an additional positive contribution of IFN- $\gamma$  cannot be excluded.<sup>34</sup>

### Diversity of microbiota determines the BPI phenotype

Pet store animals with a diverse microbiota have an immune function more comparable to human adults as opposed to laboratory mice kept in abnormally hygienic-specific pathogen-free (SPF) barrier facilities.<sup>35</sup> Therefore, we extended microbial experience by transfer of mice from SPF to conventional housing. Microbiota diversity was fostered by repeated dirty bedding. Given the impact of gut microbiota on T cell differentiation,<sup>35–37</sup> WT and *Bpi*<sup>-/-</sup> microbiota-enriched mice were continuously co-housed for 4 weeks to ensure equivalent germ exposure at the time of analysis. Indeed, principal components analysis revealed no significant difference in microbiota of caecum stools derived from co-housed WT and *Bpi*<sup>-/-</sup> mice (Figure 7A). Albeit, a significant difference for conventional as opposed to SPF conditions was apparent, along with an increased bacterial load and microbial diversity (Figures 7A–7C). Mice newly acquired 8 genera not present in SPF housing (Figure 7D). No differences were observed in frequencies of CD3<sup>+</sup> lymphocytes and CD3<sup>+</sup>CD4<sup>+</sup> T cells (Figures S8A and S8B). Yet, in comparison of WT to *Bpi*<sup>-/-</sup> mice, the proximal mLNs were enlarged with higher total cell numbers, along with a significantly increased relative and absolute amount of CD3<sup>+</sup>CD4<sup>+</sup>CD44<sup>+</sup> T cells (Figures 7E–7G; Figure S8C). Moreover, the level of IL-22 was decreased within CD3<sup>+</sup>CD4<sup>+</sup> cells

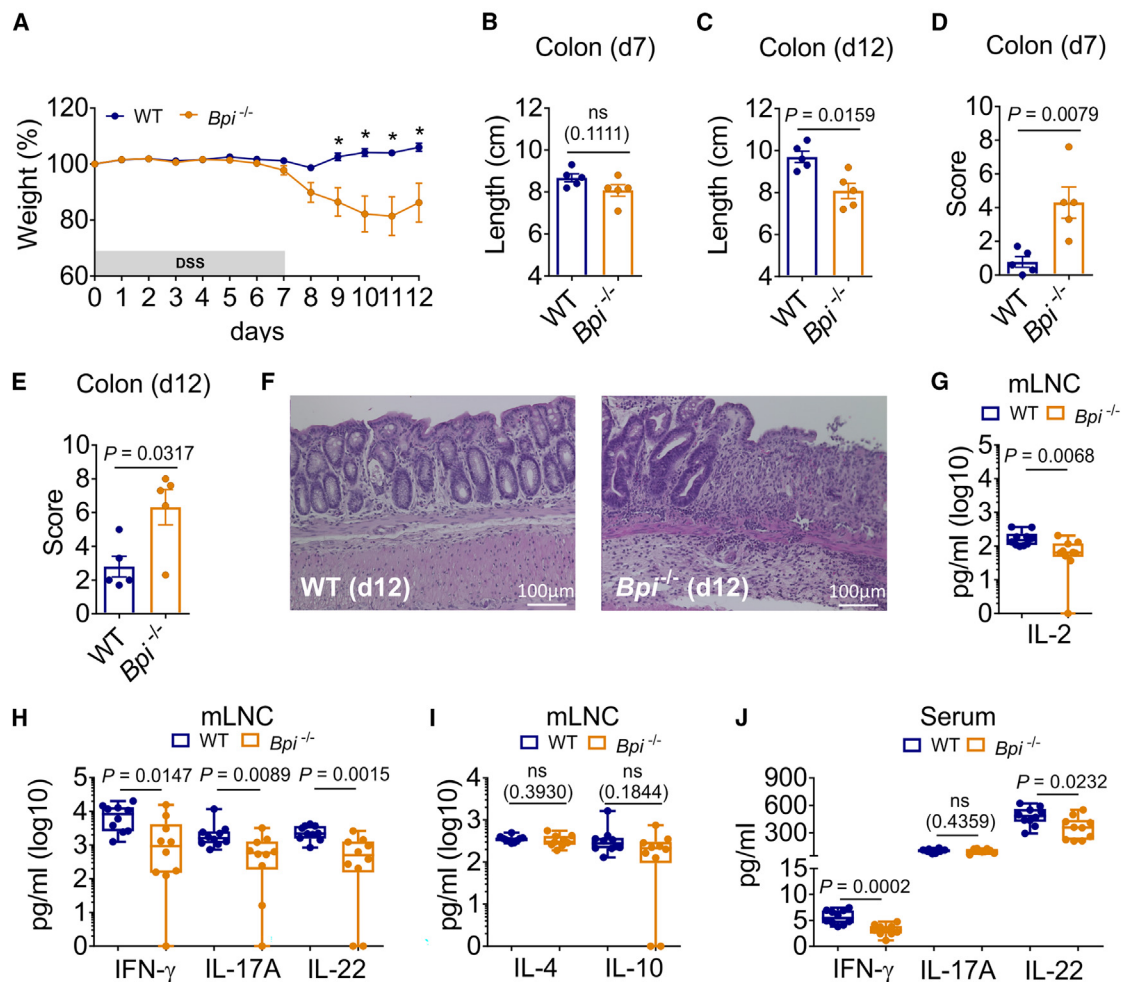


**Figure 6. BPI attenuates severity of DSS-induced colitis in mice**

(A) Relative weight of C57BL/6J WT and *Bpi*<sup>-/-</sup> mice over the course of 1.8% DSS for 7 days followed by a regeneration phase without DSS of 5 days (*n* = 10, analysis of 5 mice on d7 and d12). Statistical comparison of WT and *Bpi*<sup>-/-</sup> mice (\**p* < 0.05).

(B–F) Quantification of colon length (B and C) and histological score (D and E) on d7 and d12 as well as representative histological cross-section of the distal colon on d12 (hematoxylin and eosin stain; F) of mice shown in (A).

(G–J) Analysis of WT and *Bpi*<sup>-/-</sup> mice continuously co-housed during application of 2.5% DSS for 7 days (*n* = 10). Cytokine levels in the supernatants of mLNCS activated by αCD3 and αCD28 antibodies for 24 h (G) and 48 h (H and I). Serum levels of IFN-γ, IL-17A, and IL-22 on d7 (J). Data are depicted as median ± SEM (A–E) or boxplots showing median, upper, and lower quartiles and whiskers indicating minimal and maximal values (G–J). Statistical testing was performed using two-tailed Mann-Whitney *U* test. See also Figures S5–S7.

of mLN and in the supernatant of *ex vivo*-cultured mLNCS derived from *Bpi*<sup>-/-</sup> mice (Figures 7H and 7I). A significant BPI-dependent difference in intracellular IL-22 was also found in pLN but not in spleen cells (Figure 7I). Upon *ex vivo* culturing of the mLNCS, spontaneous IL-22 secretion was only seen in cells from WT but not *Bpi*<sup>-/-</sup> mice. Congruent with decreased IL-22 secretion by proximal mLNC in the presence of activating αCD3 and αCD28 antibodies, the respective mRNA was also decreased in mLNCS derived from *Bpi*<sup>-/-</sup> mice (Figures 7K and 7L). In accordance to the activation of BMDCs by BPI observed *in vitro* (Figures S3C and S3F), significantly higher CD86 expression was observed for CD11c<sup>+</sup>CD11b<sup>-</sup>CD103<sup>-</sup> DCs, but not in CD11c<sup>+/+</sup>CD11b<sup>high</sup>F4/80<sup>+</sup> macrophages or other DC subsets, derived from mLN of WT compared to *Bpi*<sup>-/-</sup> mice

(Figures S8D–S8H). Thus, BPI-dependent activation of mesenteric DC subsets as well as IL-22 expression in CD4<sup>+</sup> T cells is fostered by diversification of intestinal microbiota.

## DISCUSSION

BPI is a protein almost exclusively expressed in neutrophils and, according to our data, exhibits a yet undefined capacity to activate DCs. Specifically, BPI activates these cells to upregulate activation markers, including IL-2, defining BPI as a DAMP. Other DAMPs, such as lactoferrin, high-mobility group nucleosome binding domain 1, eosinophil-derived neurotoxin, or IL-33, also promote DC activation, but pronounced IL-2 production has not been described<sup>38–40</sup> or was by far lower than

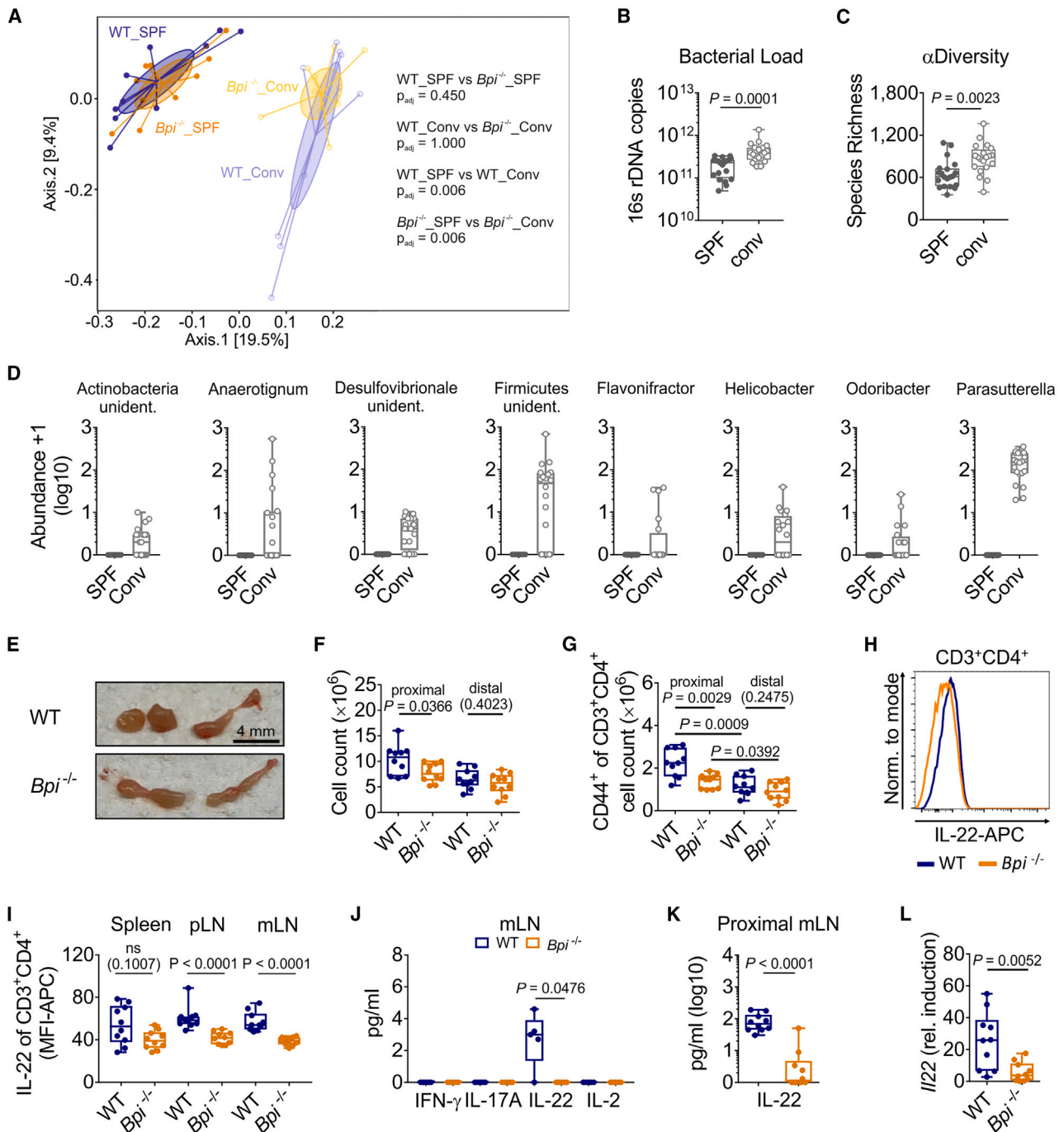


**Figure 7. BPI-mediated activation of IL-22-producing T cells *in vivo* is modulated by gut microbiota**

(A–C) C57BL/6J WT and  $Bpi^{-/-}$  mice co-housed for 4 weeks in a conventional animal facility (Conv; n = 10 per genotype and condition). Analysis of microbiota in caecum stools by principal components analysis (A). Bacterial load (B) and  $\alpha$ diversity (C) is indicated.

(D) Bacterial genera absent in SPF but present in Conv housing as revealed by DESeq2 differential abundance analysis.

(E) Representative images of proximal (left) and distal (right) mLNs from WT and  $Bpi^{-/-}$  mice.

(F and G) Counts for total (F) and CD44<sup>+</sup> of CD3<sup>+</sup>CD4<sup>+</sup> (G) mLN cells of WT and  $Bpi^{-/-}$  mice.

(H and I) Representative histogram and MFI for IL-22 in CD3<sup>+</sup>CD4<sup>+</sup> splenic, pLN, or mLN cells of WT and  $Bpi^{-/-}$  mice.

(J and K) Cytokines levels in the supernatant of mLNCs after 24 h in culture without (J; n = 5) and with activation by  $\alpha$ CD3 and  $\alpha$ CD28 antibodies (K; n = 10).

(L) Relative gene expression of *Il22* corresponding to (J). Data are depicted as boxplots showing median, upper, and lower quartiles and whiskers indicating minimal and maximal values (B–D, F, G, and I–L). Statistical testing was performed using two-tailed Mann-Whitney *U* test. See also Figure S8.

seen for BPI.<sup>41</sup> The NFATc2/c3-dependent upregulation of cytokines mediated by BPI drives secretion of tissue-protective IL-22 by CD4<sup>+</sup> T cells. These effects are strong enough to even promote Th22 differentiation in naive cells. *In vivo*, BPI deficiency results in significantly impaired IL-22 induction along with increased disease severity during DSS-induced colitis, thus explaining the defective intestinal barrier described for BPI-deficient mice during colitis.<sup>31</sup> In a broader sense, the BPI-DC-Th22 axis is of special interest in multiple diseases with known or highly suspected impact of IL-22<sup>17,30,42–44</sup> and concurrent neutrophil activation<sup>10,13,16,45</sup> such as infections including COVID-19, IBD, rheumatoid arthritis, or psoriasis. In contrast, patients undergoing allogeneic hematopoietic stem cell transplantation are lacking BPI due to neutropenia.<sup>46</sup> Since low intestinal IL-22 is an independent risk factor for mortality in these patients,<sup>19</sup> a therapeutic increase in BPI levels might ameliorate clinical outcome by fostering IL-22 expression. In mice, we could impressively induce BPI-dependent IL-22 expression in CD4<sup>+</sup> T cells by diversification of intestinal microbiota and concurrent cumulation of distinct bacterial genera. In parallel, we found a microbiota-dependent propagation of CD44<sup>+</sup> in CD3<sup>+</sup>CD4<sup>+</sup> cells in WT mice, which was abrogated in BPI deficiency, thus pointing to a central role of BPI in CD4<sup>+</sup> T cell activation. Beyond BPI, mechanisms regulating IL-22 are of general importance. Although IL-6 and TNF are known to promote Th22 induction,<sup>28</sup> we found an unexpected IL-2 dependency of IL-22 secretion, fitting the pivotal role of IL-2 on IL-22 expression in type 3 innate lymphoid cells (ILC3s).<sup>47</sup> Regarding BPI responsiveness *in vivo*, our data indicate a decisive role of CD11c<sup>+</sup>CD11b<sup>−</sup>CD103<sup>−</sup> cDCs, a cell type distinct from other intestinal CD103<sup>−</sup> cDC subsets,<sup>48</sup> which warrants further investigations. In conclusion, the neutrophil granule protein BPI substantially contributes to tissue-protective IL-22 secretion by Th22 cells via activation of cDCs. During inflammation, BPI thereby potentially counter-regulates neutrophil-mediated tissue destruction by nurturing IL-22-dependent tissue healing.

### Limitations of the study

Although most probably derived from abundantly present neutrophils during colitis, we did not exclude intestinal epithelial cells as a source of BPI.<sup>49</sup> At that point, it can only be speculated if the unexpected effects of BPI toward gram-positive bacteria seen *in vivo*<sup>31</sup> might be mediated by the bactericidal activity of antimicrobial peptides such as defensins or Reg3 lectins, which are inducible by IL-22.<sup>30,32,50,51</sup> Furthermore, a potential role of BPI in induction of IL-22 production in ILC3s was not addressed and would be of interest in further studies.

### STAR★METHODS

Detailed methods are provided in the online version of this paper and include the following:

- KEY RESOURCES TABLE
- RESOURCE AVAILABILITY
  - Lead contact
  - Materials availability

- Data and code availability
- EXPERIMENTAL MODEL AND STUDY PARTICIPANT DETAILS
  - Mice
  - Generation and purification of BPI antibodies
  - Dextran sodium sulfate colitis
  - Experiments in conventional housing
  - Cell culture
  - Isolation and stimulation of lymphocyte and dendritic cell populations
  - Ethics statement
- METHOD DETAILS
  - Cloning, production, and purification of recombinant BPI and LBP
  - Quantification of cytokine levels
  - Flow cytometry
  - RNA isolation and quantitative real-time PCR
  - Gene chip microarray assay
  - Confocal imaging
  - Immunoblot analysis
  - Microbiota analysis
- QUANTIFICATION AND STATISTICAL ANALYSIS

### SUPPLEMENTAL INFORMATION

Supplemental information can be found online at <https://doi.org/10.1016/j.celrep.2024.113929>.

### ACKNOWLEDGMENTS

We thank Ursula Holzinger, Christine Irtenkauf, Alexandra Müller, Eva-Maria Prüglmeier, Nadja Reul, Nicole Ritter, and Nadine Theissen (all Institute of Clinical Microbiology and Hygiene, University Hospital Regensburg, Germany) for their technical assistance. We also thank Dr. Joachim Gläsner (Institute of Clinical Microbiology and Hygiene, University Hospital Regensburg, Germany) and Professor Dr. Thomas Miethe (Institute of Medical Microbiology and Hygiene, University of Heidelberg, Mannheim, Germany) for advice and discussions. Moreover, we thank Prof. Dr. Michael Rehli for performing SNP analysis and Prof. Dr. Petra Hofmann for sorting naive T cells (both Department of Internal Medicine III, University Hospital Regensburg, Germany).

This work was supported by the Deutsche Forschungsgemeinschaft (DFG, project numbers 324392634-TRR 221(B13) and GE 671/14-2 to A.G.).

### AUTHOR CONTRIBUTIONS

Conceptualization – *in vitro* experiments, S.B.; conceptualization – *in vivo* experiments, S.B. and A.G.; methodology, S.B., K.U.E., J.M.H., L.Z., M.W., M.T., C.P., S.H., F.G., A.H., and A.G.; investigation, S.B., K.U.E., J.M.H., M.W., M.T., and A.G.; formal analysis, A.H.; visualization, L.Z.; writing – original draft, S.B., K.U.E., and J.M.H.; writing – review & editing, S.B. and all other authors; funding acquisition, A.G.; resources, F.B.-S. and A.G.; supervision, S.B.

### DECLARATION OF INTERESTS

K.U.E. is now a full employee of Viramed Biotech AG, Behringstr. 11, 82152 Planegg, Germany. J.M.H. is now a full employee of FUTRUE GmbH, Am Haag 14, 82166 Gräfelfing, Germany. F.G. is now a full employee of the Department of Cardiology, Pneumology and Internal Intensive Care Medicine, Hospital Neuperlach Munich, Oskar-Maria-Graf-Ring 51, 81737 Munich, Germany. The University of Regensburg is applying for a patent (PCT/EP2019/061989) covering parts published in this manuscript with A.G. and S.B. as inventors.

Received: December 21, 2022  
Revised: January 1, 2024  
Accepted: February 21, 2024

## REFERENCES

- Weiss, J., and Olsson, I. (1987). Cellular and subcellular localization of the bactericidal/permeability-increasing protein of neutrophils. *Blood* 69, 652–659.
- Skopelja, S., Hamilton, B.J., Jones, J.D., Yang, M.-L., Mamula, M., Ashare, A., Gifford, A.H., and Rigby, W.F. (2016). The role for neutrophil extracellular traps in cystic fibrosis autoimmunity. *JCI Insight* 1, e88912. <https://doi.org/10.1172/jci.insight.88912>.
- Brinkmann, V., Reichard, U., Goosmann, C., Fauler, B., Uhlemann, Y., Weiss, D.S., Weinrauch, Y., and Zychlinsky, A. (2004). Neutrophil extracellular traps kill bacteria. *Science* 303, 1532–1535. <https://doi.org/10.1126/science.1092385>.
- Weiss, J., Elsbach, P., Shu, C., Castillo, J., Grinna, L., Horwitz, A., and Theofan, G. (1992). Human bactericidal/permeability-increasing protein and a recombinant NH<sub>2</sub>-terminal fragment cause killing of serum-resistant gram-negative bacteria in whole blood and inhibit tumor necrosis factor release induced by the bacteria. *J. Clin. Invest.* 90, 1122–1130. <https://doi.org/10.1172/JCI115930>.
- Ederer, K.U., Holzinger, J.M., Maier, K.T., Zeller, L., Werner, M., Toelge, M., Gessner, A., and Bülow, S. (2022). A polymorphism of bactericidal/permeability-increasing protein affects its neutralization efficiency towards lipopolysaccharide. *Int. J. Mol. Sci.* 23, 1324. <https://doi.org/10.3390/ijms23031324>.
- Holzinger, J.M., Toelge, M., Werner, M., Ederer, K.U., Siegmund, H.I., Peterhoff, D., Blaas, S.H., Gisch, N., Brochhausen, C., Gessner, A., and Bülow, S. (2023). Scorpionfish BPI is highly active against multiple drug-resistant *Pseudomonas aeruginosa* isolates from people with cystic fibrosis. *Elife* 12, e86369. <https://doi.org/10.7554/eLife.86369>.
- Bülow, S., Zeller, L., Werner, M., Toelge, M., Holzinger, J., Entzian, C., Schubert, T., Waldow, F., Gisch, N., Hammerschmidt, S., and Gessner, A. (2018). Bactericidal/permeability-increasing protein is an enhancer of bacterial lipoprotein recognition. *Front. Immunol.* 9, 2768. <https://doi.org/10.3389/fimmu.2018.02768>.
- Bülow, S., Heyd, R., Toelge, M., Ederer, K.U., Schweda, A., Blaas, S.H., Hamer, O.W., Hiergeist, A., Wenzel, J.J., and Gessner, A. (2020). Lipopolysaccharide binding protein and bactericidal/permeability-increasing protein as biomarkers for invasive pulmonary aspergillosis. *J. Fungi* 6, 304. <https://doi.org/10.3390/jof6040304>.
- Nie, X., Qian, L., Sun, R., Huang, B., Dong, X., Xiao, Q., Zhang, Q., Lu, T., Yue, L., Chen, S., et al. (2021). Multi-organ proteomic landscape of COVID-19 autopsies. *Cell* 184, 775–791.e14. <https://doi.org/10.1016/j.cell.2021.01.004>.
- Schulte-Schrepping, J., Reusch, N., Paclik, D., Baßler, K., Schlickeiser, S., Zhang, B., Krämer, B., Krammer, T., Brumhard, S., Bonaguro, L., et al. (2020). Severe COVID-19 is marked by a dysregulated myeloid cell compartment. *Cell* 182, 1419–1440.e23. <https://doi.org/10.1016/j.cell.2020.08.001>.
- Maloy, K.J., and Powrie, F. (2011). Intestinal homeostasis and its breakdown in inflammatory bowel disease. *Nature* 474, 298–306. <https://doi.org/10.1038/nature10208>.
- Gupta, S., and Kaplan, M.J. (2021). Bite of the wolf: innate immune responses propagate autoimmunity in lupus. *J. Clin. Invest.* 131, e144918. <https://doi.org/10.1172/JCI144918>.
- Kvist-Hansen, A., Kaiser, H., Wang, X., Krakauer, M., Gortz, P.M., McCauley, B.D., Zachariae, C., Becker, C., Hansen, P.R., and Skov, L. (2021). Neutrophil Pathways of Inflammation Characterize the Blood Transcriptomic Signature of Patients with Psoriasis and Cardiovascular Disease. *Int. J. Mol. Sci.* 22, 10818. <https://doi.org/10.3390/ijms221910818>.
- Díez-Obrero, V., Moratalla-Navarro, F., Ibáñez-Sanz, G., Guardiola, J., Rodríguez-Moranta, F., Obón-Santacana, M., Díez-Villanueva, A., Dampier, C.H., Devall, M., Carreras-Torres, R., et al. (2022). Transcriptome-wide association study for inflammatory bowel disease reveals novel candidate susceptibility genes in specific colon Subsites and Tissue Categories. *J. Crohns Colitis* 16, 275–285. <https://doi.org/10.1093/ecco-jcc/jjab131>.
- Villanueva, E., Yalavarthi, S., Berthier, C.C., Hodgins, J.B., Khandpur, R., Lin, A.M., Rubin, C.J., Zhao, W., Olsen, S.H., Klinker, M., et al. (2011). Netting neutrophils induce endothelial damage, infiltrate tissues, and expose immunostimulatory molecules in systemic lupus erythematosus. *J. Immunol.* 187, 538–552. <https://doi.org/10.4049/jimmunol.1100450>.
- Phillipson, M., and Kubes, P. (2019). The healing power of neutrophils. *Trends Immunol.* 40, 635–647. <https://doi.org/10.1016/j.it.2019.05.001>.
- Ouyang, W., and O'Garra, A. (2019). IL-10 Family Cytokines IL-10 and IL-22: from Basic Science to Clinical Translation. *Immunity* 50, 871–891. <https://doi.org/10.1016/j.immuni.2019.03.020>.
- Mizoguchi, A., Yano, A., Himuro, H., Ezaki, Y., Sadanaga, T., and Mizoguchi, E. (2018). Clinical importance of IL-22 cascade in IBD. *J. Gastroenterol.* 53, 465–474. <https://doi.org/10.1007/s00535-017-1401-7>.
- Ghimire, S., Ederer, K.U., Meedt, E., Weber, D., Matos, C., Hiergeist, A., Zeman, F., Wolff, D., Edinger, M., PoECK, H., et al. (2022). Low intestinal IL22 associates with increased transplant-related mortality after allogeneic stem cell transplantation. *Front. Immunol.* 13, 857400. <https://doi.org/10.3389/fimmu.2022.857400>.
- Ponce, D.M., Alousi, A.M., Nakamura, R., Slingerland, J., Calafiore, M., Sandhu, K.S., Barker, J.N., Devlin, S., Shia, J., Giralt, S., et al. (2023). A phase 2 study of interleukin-22 and systemic corticosteroids as initial treatment for acute GVHD of the lower GI tract. *Blood* 141, 1389–1401. <https://doi.org/10.1182/blood.2021015111>.
- Schultz, H., Hume, J., Zhang, D.S., Giannini, T.L., and Weiss, J.P. (2007). A novel role for the bactericidal/permeability increasing protein in interactions of Gram-negative bacterial outer membrane blebs with dendritic cells. *J. Immunol.* 179, 2477–2484. <https://doi.org/10.4049/jimmunol.179.4.2477>.
- Helft, J., Böttcher, J., Chakravarty, P., Zelenay, S., Huotari, J., Schraml, B.U., Goubau, D., and Reis e Sousa, C. (2015). GM-CSF mouse bone marrow cultures comprise a heterogeneous population of CD11c(+) MHCII(+) macrophages and dendritic cells. *Immunity* 42, 1197–1211. <https://doi.org/10.1016/j.immuni.2015.05.018>.
- Lennartsson, A., Pieters, K., Vidovic, K., and Gullberg, U. (2005). A murine antibacterial ortholog to human bactericidal/permeability-increasing protein (BPI) is expressed in testis, epididymis, and bone marrow. *J. Leukoc. Biol.* 77, 369–377. <https://doi.org/10.1189/jlb.0304159>.
- Granucci, F., Vizzardelli, C., Pavelka, N., Feau, S., Persico, M., Virzi, E., Rescigno, M., Moro, G., and Ricciardi-Castagnoli, P. (2001). Inducible IL-2 production by dendritic cells revealed by global gene expression analysis. *Nat. Immunol.* 2, 882–888. <https://doi.org/10.1038/ni0901-882>.
- Wuest, S.C., Edwan, J.H., Martin, J.F., Han, S., Perry, J.S.A., Cartagena, C.M., Matsuura, E., Maric, D., Waldmann, T.A., and Bielekova, B. (2011). A role for interleukin-2 trans-presentation in dendritic cell-mediated T cell activation in humans, as revealed by daclizumab therapy. *Nat. Med.* 17, 604–609. <https://doi.org/10.1038/nm.2365>.
- Rogers, N.C., Slack, E.C., Edwards, A.D., Nolte, M.A., Schulz, O., Schweighoffer, E., Williams, D.L., Gordon, S., Tybulewicz, V.L., Brown, G.D., and Reis e Sousa, C. (2005). Syk-dependent cytokine induction by Dectin-1 reveals a novel pattern recognition pathway for C type lectins. *Immunity* 22, 507–517. <https://doi.org/10.1016/j.immuni.2005.03.004>.
- Zanoni, I., Ostuni, R., Capuano, G., Collini, M., Caccia, M., Ronchi, A.E., Rocchetti, M., Mingozzi, F., Foti, M., Chirico, G., et al. (2009). CD14 regulates the dendritic cell life cycle after LPS exposure through NFAT activation. *Nature* 460, 264–268. <https://doi.org/10.1038/nature08118>.
- Duhen, T., Geiger, R., Jarrossay, D., Lanzavecchia, A., and Sallusto, F. (2009). Production of interleukin 22 but not interleukin 17 by a subset of

- human skin-homing memory T cells. *Nat. Immunol.* 10, 857–863. <https://doi.org/10.1038/ni.1767>.
29. Mencarelli, A., Khameneh, H.J., Fric, J., Vacca, M., El Daker, S., Janela, B., Tang, J.P., Nabti, S., Balachander, A., Lim, T.S., et al. (2018). Calcineurin-mediated IL-2 production by CD11c<sup>high</sup>MHCII\* myeloid cells is crucial for intestinal immune homeostasis. *Nat. Commun.* 9, 1102. <https://doi.org/10.1038/s41467-018-03495-3>.
  30. Sonnenberg, G.F., Fouser, L.A., and Artis, D. (2011). Border patrol: regulation of immunity, inflammation and tissue homeostasis at barrier surfaces by IL-22. *Nat. Immunol.* 12, 383–390. <https://doi.org/10.1038/ni.2025>.
  31. Kong, Q., Lv, Z., Kang, Y., An, Y., Liu, Z., and Zhang, J. (2020). Bactericidal Permeability Increasing Protein Deficiency Aggravates Acute Colitis in Mice by Increasing the Serum Levels of Lipopolysaccharide. *Front. Immunol.* 11, 614169. <https://doi.org/10.3389/fimmu.2020.614169>.
  32. Wolk, K., Kunz, S., Witte, E., Friedrich, M., Asadullah, K., and Sabat, R. (2004). IL-22 increases the innate immunity of tissues. *Immunity* 21, 241–254. <https://doi.org/10.1016/j.immuni.2004.07.007>.
  33. Berndt, B.E., Zhang, M., Chen, G.-H., Huffnagle, G.B., and Kao, J.Y. (2007). The role of dendritic cells in the development of acute dextran sulfate sodium colitis. *J. Immunol.* 179, 6255–6262. <https://doi.org/10.4049/jimmunol.179.9.6255>.
  34. Frasch, S.C., McNamee, E.N., Kominsky, D., Jedlicka, P., Jakubzick, C., Zemski Berry, K., Mack, M., Furuta, G.T., Lee, J.J., Henson, P.M., et al. (2016). G2A Signaling Dampens Colitic Inflammation via Production of IFN- $\gamma$ . *J. Immunol.* 197, 1425–1434. <https://doi.org/10.4049/jimmunol.1600264>.
  35. Beura, L.K., Hamilton, S.E., Bi, K., Schenkel, J.M., Odumade, O.A., Casey, K.A., Thompson, E.A., Fraser, K.A., Rosato, P.C., Filali-Mouhim, A., et al. (2016). Normalizing the environment recapitulates adult human immune traits in laboratory mice. *Nature* 532, 512–516. <https://doi.org/10.1038/nature17655>.
  36. Honda, K., and Littman, D.R. (2016). The microbiota in adaptive immune homeostasis and disease. *Nature* 535, 75–84. <https://doi.org/10.1038/nature18848>.
  37. Rosshart, S.P., Herz, J., Vassallo, B.G., Hunter, A., Wall, M.K., Badger, J.H., McCulloch, J.A., Anastasakis, D.G., Sarshad, A.A., Leonardi, I., et al. (2019). Laboratory mice born to wild mice have natural microbiota and model human immune responses. *Science* 365, eaaw4361. <https://doi.org/10.1126/science.aaw4361>.
  38. De La Rosa, G., Yang, D., Tewary, P., Varadhachary, A., and Oppenheim, J.J. (2008). Lactoferrin acts as an alarmin to promote the recruitment and activation of APCs and antigen-specific immune responses. *J. Immunol.* 180, 6868–6876. <https://doi.org/10.4049/jimmunol.180.10.6868>.
  39. Yang, D., Chen, Q., Su, S.B., Zhang, P., Kurosaka, K., Caspi, R.R., Michalek, S.M., Rosenberg, H.F., Zhang, N., and Oppenheim, J.J. (2008). Eosinophil-derived neurotoxin acts as an alarmin to activate the TLR2-MyD88 signal pathway in dendritic cells and enhances Th2 immune responses. *J. Exp. Med.* 205, 79–90. <https://doi.org/10.1084/jem.20062027>.
  40. Yang, D., Postnikov, Y.V., Li, Y., Tewary, P., de la Rosa, G., Wei, F., Klinman, D., Gioannini, T., Weiss, J.P., Furusawa, T., et al. (2012). High-mobility group nucleosome-binding protein 1 acts as an alarmin and is critical for lipopolysaccharide-induced immune responses. *J. Exp. Med.* 209, 157–171. <https://doi.org/10.1084/jem.20101354>.
  41. Matta, B.M., Lott, J.M., Mathews, L.R., Liu, Q., Rosborough, B.R., Blazar, B.R., and Turnquist, H.R. (2014). IL-33 is an unconventional alarmin that stimulates IL-2 secretion by dendritic cells to selectively expand IL-33R/ST2+ regulatory T cells. *J. Immunol.* 193, 4010–4020. <https://doi.org/10.4049/jimmunol.1400481>.
  42. Hanash, A.M., Dudakov, J.A., Hua, G., O'Connor, M.H., Young, L.F., Singer, N.V., West, M.L., Jenq, R.R., Holland, A.M., Kappel, L.W., et al. (2012). Interleukin-22 protects intestinal stem cells from immune-mediated tissue damage and regulates sensitivity to graft versus host disease. *Immunity* 37, 339–350. <https://doi.org/10.1016/j.immuni.2012.05.028>.
  43. Janssen, N.A.F., Grondman, I., de Nooijer, A.H., Boahen, C.K., Koeken, V.A.C.M., Matzaraki, V., Kumar, V., He, X., Kox, M., Koenen, H.J.P.M., et al. (2021). Dysregulated Innate and Adaptive Immune Responses Discriminate Disease Severity in COVID-19. *J. Infect. Dis.* 223, 1322–1333. <https://doi.org/10.1093/infdis/jiab065>.
  44. Clinicaltrials.gov. Study of F-652 in Subjects with Corona Virus Disease 2019 (COVID-19) Pneumonia. <https://clinicaltrials.gov/ct2/show/NCT05205668>.
  45. Castanheira, F.V.S., and Kubes, P. (2019). Neutrophils and NETs in modulating acute and chronic inflammation. *Blood* 133, 2178–2185. <https://doi.org/10.1182/blood-2018-11-844530>.
  46. Zeiser, R., Socié, G., Schroeder, M.A., Abhyankar, S., Vaz, C.P., Kwon, M., Clausen, J., Volodin, L., Giebel, S., Chacon, M.J., et al. (2022). Efficacy and safety of itacitinib versus placebo in combination with corticosteroids for initial treatment of acute graft-versus-host disease (GRAVITAS-301): a randomised, multicentre, double-blind, phase 3 trial. *Lancet. Haematol.* 9, e14–e25. [https://doi.org/10.1016/S2352-3026\(21\)00367-7](https://doi.org/10.1016/S2352-3026(21)00367-7).
  47. Bauché, D., Joyce-Shaikh, B., Fong, J., Villarino, A.V., Ku, K.S., Jain, R., Lee, Y.-C., Annamalai, L., Yearley, J.H., and Cua, D.J. (2020). IL-23 and IL-2 activation of STAT5 is required for optimal IL-22 production in ILC3s during colitis. *Sci. Immunol.* 5, eaav1080. <https://doi.org/10.1126/sciimmunol.aav1080>.
  48. Cerovic, V., Houston, S.A., Scott, C.L., Aumeunier, A., Yrlid, U., Mowat, A.M., and Milling, S.W.F. (2013). Intestinal CD103<sup>+</sup> dendritic cells migrate in lymph and prime effector T cells. *Mucosal Immunol.* 6, 104–113. <https://doi.org/10.1038/mi.2012.53>.
  49. Canny, G., Levy, O., Furuta, G.T., Narravula-Alipati, S., Sisson, R.B., Serhan, C.N., and Colgan, S.P. (2002). Lipid mediator-induced expression of bactericidal/permeability-increasing protein (BPI) in human mucosal epithelia. *Proc. Natl. Acad. Sci. USA* 99, 3902–3907. <https://doi.org/10.1073/pnas.052533799>.
  50. Mukherjee, S., Zheng, H., Derebe, M.G., Callenberg, K.M., Partch, C.L., Rollins, D., Propheter, D.C., Rizo, J., Grabe, M., Jiang, Q.-X., and Hooper, L.V. (2014). Antibacterial membrane attack by a pore-forming intestinal C-type lectin. *Nature* 505, 103–107. <https://doi.org/10.1038/nature12729>.
  51. Zhao, D., Kim, Y.-H., Jeong, S., Greenson, J.K., Chaudhry, M.S., Hoefting, M., Anderson, E.R., van den Brink, M.R., Peled, J.U., Gomes, A.L., et al. (2018). Survival signal REG3 $\alpha$  prevents crypt apoptosis to control acute gastrointestinal graft-versus-host disease. *J. Clin. Invest.* 128, 4970–4979. <https://doi.org/10.1172/JCI99261>.
  52. Hodge, M.R., Ranger, A.M., Charles de la Brousse, F., Hoey, T., Grusby, M.J., and Glimcher, L.H. (1996). Hyperproliferation and dysregulation of IL-4 expression in NF-ATp-deficient mice. *Immunity* 4, 397–405. [https://doi.org/10.1016/s1074-7613\(00\)80253-8](https://doi.org/10.1016/s1074-7613(00)80253-8).
  53. Skarnes, W.C., Rosen, B., West, A.P., Koutourakis, M., Bushell, W., Iyer, V., Mujica, A.O., Thomas, M., Harrow, J., Cox, T., et al. (2011). A conditional knockout resource for the genome-wide study of mouse gene function. *Nature* 474, 337–342. <https://doi.org/10.1038/nature10163>.
  54. Caton, M.L., Smith-Raska, M.R., and Reizis, B. (2007). Notch-RBP-J signaling controls the homeostasis of CD8<sup>+</sup> dendritic cells in the spleen. *J. Exp. Med.* 204, 1653–1664. <https://doi.org/10.1084/jem.20062648>.
  55. Mähler, M., Berard, M., Feinstein, R., Gallagher, A., Ilgen-Wilcke, B., Pritchett-Corning, K., and Raspa, M. (2014). FELASA recommendations for the health monitoring of mouse, rat, hamster, guinea pig and rabbit colonies in breeding and experimental units. *Lab. Anim* 48, 178–192. <https://doi.org/10.1177/0023677213516312>.
  56. Obermeier, F., Strauch, U.G., Dunger, N., Grunwald, N., Rath, H.C., Herfarth, H., Schölmerich, J., and Falk, W. (2005). In vivo CpG DNA/toll-like receptor 9 interaction induces regulatory properties in CD4<sup>+</sup>CD62L<sup>+</sup> T cells which prevent intestinal inflammation in the SCID transfer model of colitis. *Gut* 54, 1428–1436. <https://doi.org/10.1136/gut.2004.046946>.
  57. Lutz, M.B., Kukulsch, N., Ogilvie, A.L., Rössner, S., Koch, F., Romani, N., and Schuler, G. (1999). An advanced culture method for generating large quantities of highly pure dendritic cells from mouse bone marrow.

- J. Immunol. Methods 223, 77–92. [https://doi.org/10.1016/s0022-1759\(98\)00204-x](https://doi.org/10.1016/s0022-1759(98)00204-x).
58. Mayer, C.T., Ghorbani, P., Nandan, A., Dudek, M., Arnold-Schrauf, C., Hesse, C., Berod, L., Stüve, P., Puttur, F., Merad, M., and Sparwasser, T. (2014). Selective and efficient generation of functional Batf3-dependent CD103<sup>+</sup> dendritic cells from mouse bone marrow. *Blood* 124, 3081–3091. <https://doi.org/10.1182/blood-2013-12-545772>.
59. Lutz, M.B., Ali, S., Audiger, C., Autenrieth, S.E., Berod, L., Bigley, V., Cyran, L., Dalod, M., Dörrie, J., Dudziak, D., et al. (2023). Guidelines for mouse and human DC generation. *Eur. J. Immunol.* 53, e2249816. <https://doi.org/10.1002/eji.202249816>.
60. Weischenfeldt, J., and Porse, B. (2008). Bone Marrow-Derived Macrophages (BMM): Isolation and Applications. *CSH Protoc.* 2008, pdb.prot5080. <https://doi.org/10.1101/pdb.prot5080>.
61. Borriello, F., Poli, V., Shrock, E., Spreafico, R., Liu, X., Pishesha, N., Carpenet, C., Chou, J., Di Gioia, M., McGrath, M.E., et al. (2022). An adjuvant strategy enabled by modulation of the physical properties of microbial ligands expands antigen immunogenicity. *Cell* 185, 614–629.e21. <https://doi.org/10.1016/j.cell.2022.01.009>.
62. Livak, K.J., and Schmittgen, T.D. (2001). Analysis of relative gene expression data using real-time quantitative PCR and the 2<sup>-</sup>(Delta Delta C(T)) Method. *Methods* 25, 402–408. <https://doi.org/10.1006/meth.2001.1262>.
63. Basic, M., Bolsega, S., Smoczek, A., Gläsner, J., Hiergeist, A., Eberl, C., Stecher, B., Gessner, A., and Bleich, A. (2021). Monitoring and contamination incidence of gnotobiotic experiments performed in microisolator cages. *Int. J. Med. Microbiol.* 311, 151482. <https://doi.org/10.1016/j.ijmm.2021.151482>.
64. He, B., Zhu, R., Yang, H., Lu, Q., Wang, W., Song, L., Sun, X., Zhang, G., Li, S., Yang, J., et al. (2020). Assessing the impact of data preprocessing on analyzing next generation sequencing data. *Front. Bioeng. Biotechnol.* 8, 817. <https://doi.org/10.3389/fbioe.2020.00817>.
65. Callahan, B.J., Sankaran, K., Fukuyama, J.A., McMurdie, P.J., and Holmes, S.P. (2016). Bioconductor workflow for microbiome data analysis: from raw reads to community analyses. *F1000Res.* 5, 1492. <https://doi.org/10.12688/f1000research.8986.2>.
66. Yarza, P., Richter, M., Peplies, J., Euzéby, J., Amann, R., Schleifer, K.-H., Ludwig, W., Glöckner, F.O., and Rosselló-Móra, R. (2008). The all-species living tree project: a 16S rRNA-based phylogenetic tree of all sequenced type strains. *Syst. Appl. Microbiol.* 31, 241–250. <https://doi.org/10.1016/j.syapm.2008.07.001>.

STAR★METHODS

KEY RESOURCES TABLE

REAGENT or RESOURCE	SOURCE	IDENTIFIER
<b>Antibodies</b>		
Mouse IgG1 $\alpha$ Flag (clone M2)	Sigma Aldrich	Cat# F3165; RRID:AB_259529
Mouse $\alpha$ BPI (clone 4H5)	Hycult Biotech	Cat# HM2042; RRID:AB_532909
Mouse $\alpha$ BPI (neutralizing)	This paper	N/A
$\alpha$ AhR-PE (clone T49-550)	BD Biosciences	Cat# 565711; RRID:AB_2739336
$\alpha$ CD103-APC (clone 2E7)	eBioscience	Cat# 17-1031-82; RRID:AB_1106992
$\alpha$ CD11b-VioGreen (clone REA592)	Miltenyi Biotec	Cat# 130-113-811; RRID:AB_2726328
$\alpha$ CD11c-VioBlue (clone REA754)	Miltenyi Biotec	Cat# 130-110-706; RRID:AB_2654712
$\alpha$ CD16/CD32 (clone 2.4G2)	BD Biosciences	Cat# 553142; RRID:AB_394657
$\alpha$ CD19-FITC (clone 1D3)	BD Biosciences	Cat# 553785; RRID:AB_395049
$\alpha$ CD3-APC (clone REA641)	Miltenyi Biotec	Cat# 130-122-943; RRID:AB_2801978
$\alpha$ CD3-FITC (clone 145-2C11)	BD Biosciences	Cat# 553062; RRID:AB_394595
$\alpha$ CD3-FITC (clone REA641)	Miltenyi Biotec	Cat# 130-119-758; RRID:AB_2751822
$\alpha$ CD3-PacificBlue (clone 17A2)	BioLegend	Cat# 100214; RRID:AB_493644
$\alpha$ CD40-APC (clone FGK45.5)	Miltenyi Biotec	Cat# 130-102-547; RRID:AB_2660762
$\alpha$ CD44-FITC (clone IM7)	BD Biosciences	Cat# 553133; RRID:AB_2076224
$\alpha$ CD4-PerCP (clone RM4-5)	BD Biosciences	Cat# 553052; RRID:AB_394587
$\alpha$ CD4-VioGreen (clone REA604)	Miltenyi Biotec	Cat# 130-118-693; RRID:AB_2734087
$\alpha$ CD62L-PE (clone MEL-14)	Thermo Fisher	Cat# RM4304-3
$\alpha$ CD64-PerCP-Cy5.5 (clone X54-5/7.1)	BioLegend	Cat# 139307; RRID:AB_2561962
$\alpha$ CD80-PE (clone 16-10A1)	Miltenyi Biotec	Cat# 130-102-613; RRID:AB_2659267
$\alpha$ CD86-FITC (clone PO3.3)	Miltenyi Biotec	Cat# 130-123-672; RRID:AB_2889633
$\alpha$ CD86-PE (clone GL-1)	BioLegend	Cat# 105008; RRID:AB_313151
$\alpha$ CD8-PE (clone 53-6.7)	BD Biosciences	Cat# 553033; RRID:AB_394587
$\alpha$ F4/80-APC (clone BM8)	eBioscience	Cat# 17-4801-82; RRID:AB_2784648
$\alpha$ IL-22-APC (clone IL22JOP)	Thermo Fisher	Cat# 17-7222-82; RRID:AB_10597583
$\alpha$ IL-2R $\alpha$ -APC (clone REA568)	Miltenyi Biotec	Cat# 130-120-767; RRID:AB_2752188
$\alpha$ IL-2R $\alpha$ -PE (clone PC61)	BD Biosciences	Cat# 553866; RRID:AB_395101
$\alpha$ Ly6C-PE-Cy7 (clone REA796)	Miltenyi Biotec	Cat# 130-111-918; RRID:AB_2652810
$\alpha$ Ly6G-FITC (clone 1A8)	BD Biosciences	Cat# 551460; RRID:AB_394207
$\alpha$ -murine-IgG1-PE (clone A85-1)	BD Biosciences	Cat# 550083; RRID:AB_393553
$\alpha$ -murine CD3e (clone 145-2C11)	BD Biosciences	Cat# 553057; RRID:AB_394590
$\alpha$ -murine CD28 (clone 37.51)	BD Biosciences	Cat# 553294; RRID:AB_394763
$\alpha$ IL-2 (clone S4B6)	BD Biosciences	Cat# 554375; RRID:AB_395355
isotype control (clone R35-95)	BD Biosciences	Cat# 559073; RRID:AB_479682
Jnk2 (clone 56G8)	Cell Signaling Technologies	Cat# 9258; RRID:AB_2141027
p-Jnk (Thr183 and Tyr185, clone 81E11)	Cell Signaling Technologies	Cat# 4668S; RRID:AB_823588
p38 (polyclonal)	Cell Signaling Technologies	Cat# 9212S; RRID:AB_330713
p-p38 (Thr180 and Tyr182, polyclonal)	Cell Signaling Technologies	Cat# 9211; RRID:AB_331641
Erk1/2 (polyclonal)	Cell Signaling Technologies	Cat# 9102S; RRID:AB_330744
p-Erk1/2 (Thr202 and Tyr204, clone 197G2)	Cell Signaling Technologies	Cat# 4377S; RRID:AB_331775
Mouse anti- $\beta$ -Actin (clone AC-15)	Sigma Aldrich	Cat# A5441; RRID:AB_476744
Horseradish peroxidase coupled rabbit- $\alpha$ -murine (polyclonal)	Dianova	Cat# 315-035-048; RRID:AB_2340069

(Continued on next page)

**Continued**

REAGENT or RESOURCE	SOURCE	IDENTIFIER
Horseradish peroxidase coupled donkey- $\alpha$ -rabbit (polyclonal)	Dianova	Cat# 711-035-152; RRID:AB_10015282
$\alpha$ IL-2 (clone JES6-1A12)	BD Biosciences	Cat# 554424; RRID:AB_395383
Biotinylated $\alpha$ IL-2 (clone JES6-5H4)	BD Biosciences	Cat# 554426; RRID:AB_395384
$\alpha$ IL-12p40/p70 (clone C15.6)	BD Biosciences	Cat# 551219; RRID:AB_394097
Biotinylated $\alpha$ IL-12p40/p70 (clone C17.8)	BD Biosciences	Cat# 554476; RRID:AB_395419
$\alpha$ IL-17A (clone TC11-18H10)	BD Biosciences	Cat# 555068; RRID:AB_398587
Biotinylated $\alpha$ IL-17A (clone TC11-8H4)	BD Biosciences	Cat# 555067; RRID:AB_395681
$\alpha$ CCL2 (clone 2H5)	BD Biosciences	Cat# 551217; RRID:AB_394095
Biotinylated $\alpha$ CCL2 (clone 4E2/MCP)	BD Biosciences	Cat# 554444; RRID:AB_395395
$\alpha$ IFN- $\gamma$ (clone 37801/37875)	R&D Systems	Cat# MAB785; RRID:AB_2123045
Biotinylated $\alpha$ IFN- $\gamma$ (clone XMG1.2)	BD Biosciences	Cat# 554410; RRID:AB_395374

**Chemicals, peptides, and recombinant proteins**

Streptavidin-PE	Agilent	Cat# AGPJRS20-1
7-AAD	eBioscience	Cat# 00-6993-50
Brefeldin A	eBioscience	Cat# 00-4506-51
Fixable Viability Stain 780	BD Bioscience	Cat# 565388; RRID:AB_2869673
Collagenase	Sigma Aldrich	Cat# CO130
Dispase II	Sigma Aldrich	Cat# D4693
DNase I	Sigma Aldrich	Cat# DN25
( <i>R</i> )-Pam <sub>3</sub> CSK <sub>4</sub>	EMC Microcollections	Cat# L2048
BPI <sub>N</sub> (Human Neutrophil)	Athens Research and Technology	Cat# 16-14-021609
Chicken egg ovalbumin peptide 323-339	Invivogen	Cat# vas-isq
Human and murine BPI	This paper	N/A
Human LBP	This Paper	N/A
Recombinant human FLT3L	Thermo Fisher	Cat# 300-19
Ultra-Pure LPS (E. coli O111:B4)	Invivogen	Cat# tlrl-3pelps
Zymosan depleted	Invivogen	Cat# tlrl-zyd
11R-VIVIT (NFAT inhibitor)	Tocris	Cat# 3930
2-APB (IP3R inhibitor)	Abcam	Cat# ab120124
Cyclosporin A (calcineurin inhibitor)	Sigma Aldrich	Cat# 30024
PD98059 (MEK1 inhibitor)	Cell Signaling Technology	Cat# 9900
R406 (Syk inhibitor)	Selleckchem	Cat# S2194
SB203580 (p38 inhibitor)	Selleckchem	Cat# S1076
Sotrastaurin (PKC inhibitor)	Selleckchem	Cat# S2791
SP600125 (JNK inhibitor)	Selleckchem	Cat# S1460
U73122 (PLC inhibitor)	Selleckchem	Cat# S8011
UO126 (MEK1/2 inhibitor)	Promega	Cat# V1121
Flag-Peptide	peptides&elephants	Cat# EP01741
LightCycler 480 SYBR Green I Master	Roche	Cat# 4707516001
ActinGreen	Thermo Fisher	Cat# R37110
Methanol-free formaldehyde	Thermo Fisher	Cat# 28906
Dextran Sodium Sulfate (DSS)	MP Biomedicals	Cat# 216011090
cOmplete protease inhibitor cocktail	Roche	Cat# 05892970001
PhosSTOP phosphatase inhibitor cocktail	Roche	Cat# 04906837001

**Critical commercial assays**

IL-10 ELISA Set	BD Biosciences	Cat# 555252; RRID:AB_2869052
IL-22 ELISA Kit	Thermo Fisher	Cat# 88-7422-88; RRID:AB_2575121

(Continued on next page)

**Continued**

REAGENT or RESOURCE	SOURCE	IDENTIFIER
IL-23 ELISA Set	R&D Systems	Cat# DY1887
IL-6 ELISA Set	BD Biosciences	Cat# 555240; RRID:AB_2869049
TNF ELISA Set	BD Biosciences	Cat# 558534; RRID:AB_2869215
IFN- $\gamma$ Secretion Assay	Miltenyi Biotec	Cat# 130-090-516
IL-17A Secretion Assay	Miltenyi Biotec	Cat# 130-094-205
IL-2 Secretion Assay	Miltenyi Biotec	Cat# 130-090-491
Transcription Factor Buffer Set	BD Biosciences	Cat# 562574; RRID:AB_2869424
DC-Protein Assays	Bio-Rad Laboratories	Cat# 500-0111
ExpiFectamine™ 293 Transfection Kit	Thermo Fisher Scientific	Cat# A14524
GeneChip™ Mouse Gene 2.0 ST Array	Affymetrix	Cat# 902118
iScript™ Advanced cDNA Synthesis Kit	Bio-Rad Laboratories	Cat# 1725038
RNeasy Mini Kit	QIAGEN	Cat# 74106
TURBO DNA-free™ Kit	Thermo Fisher	Cat# AM1907
Monolith NT™ Protein Labeling Kit RED-NHS	NanoTemper Technologies	Cat# MO-L011

**Experimental models: Cell lines**

Expi293F™ cells	Thermo Fisher Scientific	Cat# A14527
-----------------	--------------------------	-------------

**Experimental models: Organisms/strains**

B6.129P2(SJL)-Myd88 <sup>tm1.1Defr</sup> /J	The Jackson Laboratory	Strain#: 009088, RRID: IMSR_JAX:009088
B6.Cg-Tg(TcraTcrb)425Cbn/J (OT-II)	The Jackson Laboratory	Strain#:004194, RRID: IMSR_JAX:004194
B6.C-Tg(CMV-cre)1Cgn/J (CMV-cre)	The Jackson Laboratory	Strain#:006054, RRID: IMSR_JAX:006054
<i>Bpi</i> <sup>-/-</sup>	This paper	N/A
C3H/HeJ	The Jackson Laboratory	Strain#: 000659, RRID: IMSR_JAX:000659
C57BL/6J	The Jackson Laboratory	Strain#:000664, RRID: IMSR_JAX:000664
<i>Cd11c-cre</i>	Professor Dr. Boris Reizis	N/A
<i>Nfatc2</i> <sup>-/-</sup>	Professor Dr. Laurie H. Glimcher	N/A
<i>Nfatc3</i> <sup>tm1a(EUCOMM)Hmgu</sup> ( <i>Nfatc3</i> <sup>fl/fl</sup> )	EUCOMM project	EMMA strain ID: 08102
<i>Nfatc3</i> <sup>fl/fl</sup> : <i>Cd11c-cre</i> mice ( <i>Nfatc3</i> <sup>-/-</sup> )	University of Würzburg	N/A
<i>Nfatc2</i> <sup>-/-</sup> : <i>Nfatc3</i> <sup>fl/fl</sup> : <i>Cd11c-cre</i> mice ( <i>Nfatc2c3</i> <sup>-/-</sup> )	University of Würzburg	N/A

**Oligonucleotides**

Primers for <i>Hprt</i> , see Table S1	Biomers	N/A
Primers for <i>Irfng</i> , see Table S1	Thermo Fisher	N/A
Primers for <i>Il12a</i> , see Table S1	Biomers	N/A
Primers for <i>Il12b</i> , see Table S1	Thermo Fisher	N/A
Primers for <i>Il17a</i> , see Table S1	Biomers	N/A
Primers for <i>Il2</i> , see Table S1	Microsynth	N/A
Primers for <i>Il22</i> , see Table S1	Biomers	N/A
Primers for <i>Il23a</i> , see Table S1	Thermo Fisher	N/A
Primers for <i>Il6</i> , see Table S1	Thermo Fisher	N/A
Primers for <i>Tnf</i> , see Table S1	Thermo Fisher	N/A

**Recombinant DNA**

pCR3 vector	Invitrogen	N/A
-------------	------------	-----

**Software and algorithms**

GraphPad Prism, version 7	GraphPad Software	N/A
LiquiChip Analyzer Software	QIAGEN	N/A
FlowJo v.10	BD Biosciences	N/A
SDS software version 2.4	Thermo Fisher	N/A
Leica Application Suite, version 2.7.3.9723	Leica	N/A
ChemoStar software	Intas Scienc Imaging Instruments	N/A

(Continued on next page)

<b>Continued</b>		
REAGENT or RESOURCE	SOURCE	IDENTIFIER
All-Species Living Tree Project (LTP) reference database release 12_2020	<a href="https://imedea.uib-csic.es/mmg/ftp/">https://imedea.uib-csic.es/mmg/ftp/</a>	N/A
phyloseq v1.36	Bioconductor 3.13	N/A
DESeq2 v1.31.16	Bioconductor 3.13	N/A
dada2 v1.20	Bioconductor 3.13	N/A
Trimmomatic v0.39	Github: usadellab/Trimmomatic	N/A
Cutadapt v3.4	Github: marcelm/cutadapt	N/A
<b>Other</b>		
Dulbecco's phosphate-buffered saline	Sigma Aldrich	Cat# D8537
Heat-inactivated FCS	Sigma Aldrich	Cat# F7524
Penicillin-Streptomycin	PAN-Biotech	Cat# P06-07100
StableCell™ RPMI 1640	Thermo Fisher	Cat# R2405
β-Mercaptoethanol	AppliChem	Cat# A1108
Amicon Ultra-15, PLGC Ultracel-PL Membran, 10 kDa	Merck Millipore	Cat# UFC901008
HighLoad 16/600Superdex 75 pg column	Cytiva	Cat# 28989333
HiTrap™ SP HP column	Cytiva	Cat# 17115101
NHS-activated HP column	Cytiva	Cat# 17071701
70 μm cell strainers	Sarstedt	Cat# 83.3945.070
FACS Aria™ II	BD Biosciences	N/A
IMDM medium	PAN-Biotech	Cat# P04-20150
Naive CD4 <sup>+</sup> T cell Isolation Kit, mouse	Miltenyi Biotec	Cat# 130-104-453
Luminex® 100 system	Luminex corp.	N/A
BD FACSCanto™ II	BD Bioscience	N/A
ABI PRISM® 7900HT Sequence Detection System	Thermo Fisher	N/A
LightCycler® 480II	Roche	N/A
QIAshredder homogenizer columns	QIAGEN	Cat# 79656
μ-Slide VI 0.5 Glass Bottom	ibidi	Cat# 80607
Leica TCS SP5 confocal laser microscope	Leica	N/A
Mounting medium containing DAPI	ibidi	Cat# 50011
ChemoStar Imager	Intas Sciene Imaging Instruments	N/A
Trans-Blot® Turbo™ Transfer System	Bio-Rad Laboratories	N/A
HiTrap Protein An HP antibody purification column	Cytiva	Cat# 17-0402-01
HiTrap Protein G HP antibody purification column	Cytiva	Cat# 17-0404-01
IonChef™ instrument	Thermo Fisher	N/A
IonTorrent™ Genestudio S5 Plus sequencer	Thermo Fisher	N/A

## RESOURCE AVAILABILITY

### Lead contact

Further information and requests for resources and reagents should be directed to and will be fulfilled by the lead contact, Sigrid Bülow ([sigrid.buelow@ukr.de](mailto:sigrid.buelow@ukr.de)).

### Materials availability

Mouse lines and BPI variants generated in this study will be made available on request from the [lead contact](#), but may require completed materials transfer agreement.

### Data and code availability

- The authors declare that the main data supporting the findings of this study are available within the article and its Supplementary Information files. Extra data are available from the [lead contact](#) upon request.
- This paper does not report original code.
- Any additional information required to reanalyze the data reported in this work paper is available from the [lead contact](#) upon request.

## EXPERIMENTAL MODEL AND STUDY PARTICIPANT DETAILS

### Mice

All mice were bred under SPF conditions unless indicated otherwise. SPF conditions included HEPA-filtered air under positive pressure and cages covered with microisolation filter tops. Mice were allowed free access to de-ionized water and commercial diet, which were both autoclaved. C57BL/6J, C3H/HeJ, B6.129P2(SJL)-Myd88<sup>tm1.1Defr</sup>/J, B6.C-Tg(CMV-cre)1Cgn/J (CMV-cre) and B6.Cg-Tg(TcraTcrb)425Cbn/J (OT-II) mice were obtained from the Jackson Laboratory (Bar Harbor, ME, USA) and bred in the animal facility of the University Hospital Regensburg. *Nfatc2*<sup>-/-</sup> mice were kindly provided by Professor Dr. Laurie H. Glimcher.<sup>52</sup> The *Nfatc3*<sup>fl/fl</sup> mice were received from the EUCOMM project as *Nfatc3*<sup>tm1a(EUCOMM)Hmgu</sup><sup>53</sup> and crossed to Flp mice to generate the *Nfatc3*<sup>tm1c</sup> variant, i.e., *Nfatc3*<sup>fl/fl</sup>. *Cd11c*-cre transgene mice were kindly provided by Professor Dr. Boris Reizis.<sup>54</sup> *Nfatc3*<sup>fl/fl</sup>:*Cd11c*-cre, *Nfatc2*<sup>-/-</sup>:*Nfatc3*<sup>fl/fl</sup>:*Cd11c*-cre and corresponding *Cd11c*-cre mice (wild type, WT) were bred at the animal facility of the University of Würzburg, Germany.

To generate BPI-deficient mice, we designed a targeting vector that substituted exon three and four of the *Bpi* gene with a neomycin resistance flanked by two loci of X-over P1 (*loxP*) sites (Figure S6A). The targeting vector was introduced into embryonic stem cells (ESCs) by electroporation. ESCs that underwent recombination, indicated by resistances to neomycin and ganciclovir, were screened for the recombinant locus by Southern blot analysis (Figures S6B and S6D). In more detail, purified DNA from WT ESCs or recombinant ESCs was digested by EcoRI or BamHI, separated by electrophoresis and blotted onto a nitrocellulose membrane. Fragments matching the expected sizes for digestion with EcoRI and BamHI were visualized by a radioactive probe, which was amplified by the primer pair: 5' GTT GTC ACT GAG AGG TGG TGC 3' and 5' CTC TGG AGG CAG CAG AAG AGA 3'.

Recombinant ESCs were then injected into C57BL/6 blastocysts and transferred into pseudopregnant mice by blastocyst microinjection. Male heterozygous offspring chimera were mated with B6.C-Tg(CMV-cre)1Cgn/J mice to produce *Bpi*<sup>-/-</sup> mice (Figure S6C). Germline transmission of the knockout locus in chimeras was analyzed by PCR (Figure S6E), using primers indicated by black arrows (Figures S6A and S6C). Total knockout of *Bpi* was confirmed by reverse transcription polymerase chain reaction (RT-PCR), displaying a truncated PCR product for *Bpi*<sup>-/-</sup> mice (Figure S6F). The *Bpi* WT locus was amplified by primer pair: 5' GGG CTC TGA GGG AGG CAC CAT 3' and 5' GTG GAG ATG GAG ACG CCC TGG 3'. The locus in *Bpi*<sup>-/-</sup> mice was amplified using the primers: 5' GTG CCA GCA GGG AGT GGT TGA GTT 3' and 5' AGG CCC TGC CCC TCG CAC AC 3'. Primers used for RT-PCR were: 5' GGA TCC GGT TCA GCC ACT TCA CG 3' and 5' GCA CAG GGC CCC GGT ACA CAG AT 3'. Expression of BPI in testis of WT and *Bpi*<sup>-/-</sup> mice was analyzed by western blot analysis. Rat  $\alpha$ -murine BPI monoclonal antibody was produced by Dr. Elisabeth Kremer (Helmholtz Zentrum München, Munich, Germany; Figure S6G). Mice were back-crossed to a pure C57BL/6J background according to analysis of 122 single nucleotide polymorphisms distinguishing C57BL/6J and C57BL/6N kindly performed by Prof. Dr. Michael Rehli (Department of Internal Medicine III, University Hospital Regensburg, Germany).

### Generation and purification of BPI antibodies

Male mice were immunized with recombinant BPI<sub>F</sub> by Davids Biotechnology (Regensburg, Germany) to generate hybridoma clones. These clones were screened by ELISA for production of antibodies directed against human BPI. Positive IgG clones were selected for expansion and antibodies were purified via HiTrap Protein An HP and HiTrap Protein G HP antibody purification columns (Cytiva Europe GmbH, Freiburg, Germany).

### Dextran sodium sulfate colitis

For the induction of acute colitis with DSS, age- and weight-matched three to four months old female C57BL/6J *Bpi*<sup>-/-</sup> mice were exposed to DSS (MP Biomedicals, Eschwege, Germany) in drinking water at the indicated concentrations for seven days. In transfer experiments, 10<sup>6</sup> BMDCs were injected into the tail vein of *Bpi*<sup>-/-</sup> mice on day one of DSS exposure according to a protocol published by Berndt et al.<sup>33</sup> Mice were weighted daily. Mice were sacrificed by CO<sub>2</sub> euthanasia and cervical dislocation on day seven of acute DSS-induced colitis or five days after withdrawal of DSS. Serum was obtained for Luminex analysis and mLNCS for *ex vivo* stimulation and flow cytometry staining. For histological scoring, cross-sections of the distal colon were fixed in 10% buffered formalin and stained with hematoxylin and eosin (HE). Histological damage in intestinal tissue was quantified by 2 investigators in a blinded fashion using a previously described scoring system.<sup>55</sup>

### Experiments in conventional housing

To facilitate diverse microbial experience in indicated experiments, two month old female C57BL/6J and *Bpi*<sup>-/-</sup> mice were transferred to conventional housing conditions for four weeks. In contrast to the SPF facility, mice were exposed to non-filtered air under

atmospheric pressure and were allowed free access to tap water and commercial chow, which both were non-autoclaved. Furthermore, dirty bedding was applied with weekly addition of approximately 10% bedding used previously by mice within the conventional animal facility. Serological screen (BioDoc, Biomedical Diagnostics, Hannover, Germany) of two representative WT and *Bpi*<sup>-/-</sup> mice, culture results of pooled caecum stools (Institute of Clinical Microbiology and Hygiene, Regensburg, Germany) were negative for bacteria and viruses according to FELASA criteria.<sup>56</sup> Microbiota analysis of mice in conventional but not SPF housing revealed presence of *Helicobacter mastomyrinus* not listed in the FELASA criteria.<sup>56</sup> Routine health monitoring within the conventional animal facility was negative for endo- and ectoparasites (Envigo, Horst, Netherlands).

### Cell culture

Cells were maintained in RPMI 1640 (Thermo Fisher Scientific, Waltham, MA, USA) supplemented with 10% heat-inactivated FCS (Sigma Aldrich, Taufkirchen, Germany), 10% penicillin, 10% streptomycin (both PAN-Biotech, Aidenbach, Germany) and 50  $\mu$ M  $\beta$ -mercaptoethanol (AppliChem, Darmstadt, Germany). For generation of BMDCs, BMDMs, cDCs and PLCs three to four month old male mice were used. For BMDC generation, bone marrow cells were plated in medium supplemented with supernatant of GM-CSF producing X63 cells. Fresh medium was added on days three and six. Loose as well as semi-adherent cells were harvested on day seven or eight.<sup>57</sup> Generation of conventional type 1 DC from mouse bone marrow was performed as described previously using recombinant human FLT3L (Thermo Fisher Scientific, Waltham, MA, USA) and supernatant of GM-CSF producing X63 cells.<sup>58,59</sup> BMDMs were differentiated in the presence of L929-generated CSF-1 by plating bone marrow cells, transferring loose cell in a new Petri dish on day one, adding fresh media on day five and harvesting cells on day seven.<sup>60</sup> To obtain murine PLCs, peritonea of euthanized mice were injected with 10 mL of sterile cold PBS and massaged thoroughly. The cell suspension was then withdrawn, centrifuged (300 x g, 8 min, 4°C) and washed twice with cold PBS. For protein secretion analyses, BMDCs were seeded and stimulated with 200 nM BPI, 200 nM LBP, 10 ng/mL LPS, 10 nM bLP or 5  $\mu$ g/mL Zymd for 18 h. Unless indicated otherwise, stimulations were performed with human BPI purified via  $\alpha$ Flag columns. For inhibition experiments, R406 (2 h, 1  $\mu$ M), SB203580 (1 h, 20  $\mu$ M), SP600125 (1 h, 20  $\mu$ M), Sotrastaurin (1 h, 10  $\mu$ M) and U73122 (1 h, 1  $\mu$ M) were purchased from Selleckchem (Houston, TX, USA). 2-APB (30 min, 100  $\mu$ M) was from Abcam (Berlin, Germany), 11R-VIVIT (1 h, 5  $\mu$ M) from Tocris (Bristol, United Kingdom), CsA (30 min, 0.1  $\mu$ M) from Sigma Aldrich (Taufkirchen, Germany), PD98059 (1 h, 10  $\mu$ M) from Cell Signaling Technology (Frankfurt am Main, Germany) and UO126 (1 h, 5  $\mu$ M) from Promega (Mannheim, Germany).

### Isolation and stimulation of lymphocyte and dendritic cell populations

For preparation of lymphocytes from spleen, mLN and pLN two to three month old male C57BL/6J WT or *Bpi*<sup>-/-</sup> mice were used. Spleen, mLN and pLN cells were isolated by 70  $\mu$ m cell strainers (Sarstedt, Nümbrecht, Germany). SCs were additionally treated with red blood cell lysis buffer (150 mM NH<sub>4</sub>Cl, 10 mM KHCO<sub>3</sub>, 0.1 mM EDTA). CD4<sup>+</sup> T cells were isolated from pooled murine spleen and/or peripheral lymph nodes by negative magnetic-activated cell sorting (Miltenyi Biotec, Bergisch Gladbach, Germany). Purity of CD3<sup>+</sup>CD4<sup>+</sup> cells was 96.0%  $\pm$  0.7%.

For isolation of naive CD4<sup>+</sup> T cells, the enriched CD4<sup>+</sup> T cell fraction was stained with  $\alpha$ CD4-PerCP (RM4-5),  $\alpha$ CD44-FITC (IM7, both from BD Bioscience, Heidelberg, Germany)  $\alpha$ IL-2R $\alpha$ -APC (REA568, Miltenyi Biotec, Bergisch Gladbach, Germany) and  $\alpha$ CD62L-PE (MEL-14; Thermo Fisher Scientific, Waltham, MA, USA) antibodies. Fluorescence-activated cell sorting was performed at the Leibniz Institute for Immunotherapy (Regensburg, Germany) with the FACS Aria II (BD Biosciences, Heidelberg, Germany). Purity of naive CD4<sup>+</sup> T cells was >99.0%.

Stimulatory supernatants of BMDCs (SN BPI) and supernatant of untreated BMDCs (SN NT) were obtained after 18 h of stimulation with BPI or medium, respectively. For polyclonal activation, CD4<sup>+</sup> T cells were seeded in  $\alpha$ -murine CD3e ( $\alpha$ CD3; 145-2C11; NA/LE; BD Biosciences, Heidelberg, Germany) precoated wells and supplemented with  $\alpha$ -murine CD28 ( $\alpha$ CD28; 37.51; NA/LE; BD Biosciences, Heidelberg, Germany). IL-2 in SN BPI and SN NT was neutralized by incubation with  $\alpha$ -murine IL-2 at 1  $\mu$ g/mL ( $\alpha$ IL-2; S4B6) or the corresponding isotype control (R35-95), purchased from BD Bioscience (Heidelberg, Germany).

For OT-II T cell assays, CD4<sup>+</sup> T cells from two to three month old male OT-II mice were used. GM-CSF-derived BMDCs were incubated with chicken egg ovalbumin peptide 323–339 (OVA, 1  $\mu$ g/mL; Invivogen, Toulouse, France). BMDCs were stimulated with 400 nM BPI for 18 h for flow cytometry or cytokine readouts, respectively, before CD4<sup>+</sup> OT-II T cells were added at a ratio of 10:1. The co-culture setups were incubated for 16 h for analysis of surface markers or 24 h for cytokine quantification and analysis of transcription factors.

For analysis of DC subsets mLN from two to three month old female C57BL/6J WT or *Bpi*<sup>-/-</sup> mice were enzymatically digested according to a protocol modified from Boriello et al.<sup>61</sup> Briefly, mLN were slowly injected with 400  $\mu$ L of digestion solution consisting of IMDM medium (PAN-Biotech, Aidenbach, Germany) with 1% penicillin and streptomycin (both PAN-Biotech, Aidenbach, Germany), 2% heat-inactivated FCS (Sigma Aldrich Taufkirchen, Germany), 1 mg/mL dispase II (Sigma Aldrich Taufkirchen, Germany), 1 mg/mL collagenase (Sigma Aldrich Taufkirchen, Germany) and 0.1 mg/mL DNase I (Sigma Aldrich Taufkirchen, Germany). mLN were incubated for 20 min in the 400  $\mu$ L digestion solution at 37°C and then mechanically disrupted by repeated pipetting. Supernatants were collected and kept on ice, while 200  $\mu$ L of fresh digestion solution were added to the remaining mLN fragments and incubated for 10 min at 37°C. The last digestion step was repeated one more time. After collection of the pooled supernatants through 70  $\mu$ m cell strainers (Sarstedt, Nümbrecht, Germany) the isolated cells were washed once with fresh medium and further processed for flow cytometry.

### Ethics statement

This study was carried out in accordance with the recommendations of the Declaration of Helsinki. Animal studies were approved by the Regierung von Unterfranken (Würzburg, Germany, Az. 55.2-2532-50 and 55.2.2-2532-2-1301).

### METHOD DETAILS

#### Cloning, production, and purification of recombinant BPI and LBP

Human and murine BPI and LBP were generated as described previously<sup>7</sup> with slight modifications. In brief, huBPI (aa 32–487), muBPI (aa 28–483) and huLBP (aa 26–481), each containing a C-terminal Flag, were cloned into pCR3 vector (Thermo Fisher Scientific, Waltham, MA, USA). Expi293F cells were transfected using the ExpiFectamine 293 Transfection Kit (Thermo Fisher Scientific, Waltham, MA, USA). The expressed protein was purified by affinity chromatography on an  $\alpha$ Flag (M2; Sigma Aldrich, Taufkirchen, Germany) coupled NHS-activated HP column (Cytiva, Marlborough, MA, USA), eluted with Flag-Peptide (peptides&elephants, Berlin, Germany), concentrated via ultrafiltration (Amicon Ultracel-PL, Merck Millipore, Darmstadt, Germany) and dialyzed against PBS. The concentration was determined by DC-Protein Assays (Bio-Rad Laboratories, Feldkirchen, Germany). In addition, indicated batches were purified by cation exchange chromatography via a HiTrap SP HP column (Cytiva, Marlborough, MA, USA). Fractions containing the protein of interest were pooled and further purified by size exclusion chromatography using a HighLoad 16/600Superdex 75 pg column (Cytiva, Marlborough, MA, USA). All *in vitro* experiments were conducted with huBPI unless indicated otherwise.

#### Quantification of cytokine levels

To analyze concentrations of cytokines in cell culture supernatant and serum, Luminex technology (Austin, TX, USA) was used. Antibodies to analyze IL-2 (capture  $\alpha$ IL-2 JES6-1A12 and detection  $\alpha$ IL-2 JES6-5H4), IL-6 (IL-6 ELISA Set), IL-10 (IL-10 ELISA Set), IL-12B (capture  $\alpha$ IL-12p40/p70 C15.6 and detection  $\alpha$ IL-12p40/p70 C17.8), IL-17A (capture  $\alpha$ IL-17A TC11-18H10 and detection  $\alpha$ IL-17A TC11-8H4), CCL2 (capture  $\alpha$ CCL2 2H5 and detection  $\alpha$ CCL2 4E2/MCP) and TNF (TNF ELISA Set) were purchased from BD Bioscience (Heidelberg, Germany). IFN- $\gamma$  was detected with capture  $\alpha$ IFN- $\gamma$  (37801/37875, R&D Systems, Minneapolis, MN, USA) and detection  $\alpha$ IFN- $\gamma$  (XMG1.2, BD Biosciences, Heidelberg, Germany), IL-22 with IL-22 ELISA Kit (Thermo Fisher Scientific, Waltham, MA, USA) and IL-23 with IL-23 ELISA Set (R&D Systems, Minneapolis, MN, USA). For detection Streptavidin-PE was used (Agilent, Palo Alto, CA, USA). Samples were measured with the Luminex 100 system and analyzed by using LiquiChip Analyzer Software (QIAGEN, Hilden, Germany).

#### Flow cytometry

Staining was performed with ice-cold PBS with 1% FCS and 0.05% NaN<sub>3</sub>. For measuring BPI association to the cell surface, BMDCs were incubated for 30 min on ice with 100 nM BPI. Fc receptors were blocked by  $\alpha$ CD16 and  $\alpha$ CD32 (2.4G2, BD Biosciences, Heidelberg, Germany). BPI binding was detected either by mouse-IgG1  $\alpha$ Flag (M2, Sigma Aldrich, Taufkirchen, Germany) or mouse  $\alpha$ BPI (4H5, Hycult Biotech, Uden, Netherlands) in combination with  $\alpha$ -murine-IgG1-PE (A85-1, BD Biosciences, Heidelberg, Germany). For cell surface staining cells were stained with  $\alpha$ CD11c-VioBlue (REA754),  $\alpha$ CD11b-VioGreen (REA592),  $\alpha$ CD80-PE (16-10A1),  $\alpha$ CD86-FITC (PO3.3),  $\alpha$ CD40-APC (FGK45.5) or  $\alpha$ IL-2R $\alpha$ -APC (REA568) from Miltenyi Biotec (Bergisch Gladbach, Germany). Viability staining was performed with 7-AAD (eBioscience, Santa Clara, CA, USA).

Secretion assays were performed according to the manufacturer's instructions (Miltenyi Biotec, Bergisch Gladbach). For IL-2 secretion assay, BMDCs were stimulated with 200 nM BPI for 3 h. For IFN- $\gamma$  and IL-17A secretion assays, pooled murine spleen and pLN cells were seeded into  $\alpha$ CD3 coated wells and incubated with SN BPI or SN NT and  $\alpha$ CD28 antibodies for 16 h. Intracellular staining of transcription factors and IL-22 in T cells was performed with Transcription Factor Buffer Set (BD Bioscience, Heidelberg, Germany) according to the manufacturer's protocol. For intracellular staining of IL-22, CD4<sup>+</sup> T cells were seeded into  $\alpha$ CD3 coated wells and incubated with SN BPI or SN NT and  $\alpha$ CD28 antibodies for 24 h or 72 h. For 72 h incubation, cells were split in two wells after 48 h and resupplied with SN BPI or SN NT for 24 h. For the final 5 h of incubation, Brefeldin A (eBioscience, Santa Clara, CA, USA) was added. Cells were permeabilized and stained with  $\alpha$ CD3-FITC (145-2C11),  $\alpha$ CD4-PerCP (RM4-5), both from BD Bioscience (Heidelberg, Germany), and  $\alpha$ IL-22-APC (IL22JOP, Thermo Fisher Scientific, Waltham, MA, USA). For analysis of surface markers and intracellular staining of T cell transcription factors cells were stained with  $\alpha$ CD3-APC (REA641),  $\alpha$ CD4-VioGreen (REA604) from Miltenyi Biotec (Bergisch Gladbach, Germany), with  $\alpha$ CD8-PE (53-6.7),  $\alpha$ CD44-FITC (IM7),  $\alpha$ CD4-PerCP (RM4-5),  $\alpha$ IL-2R $\alpha$ -PE (PC61) and  $\alpha$ AhR-PE (T49-550) from BD Bioscience (Heidelberg, Germany) and  $\alpha$ IL-22-APC (IL22JOP) from Thermo Fisher Scientific (Waltham, MA, USA) and with  $\alpha$ CD3-PacificBlue (17A2) from BioLegend (Santa Clara, CA, USA).

For analysis of DC subsets in mLN, surface markers of cells gained after enzymatic digestion were stained with  $\alpha$ CD3-FITC (REA641),  $\alpha$ Ly6C-PE-Cy7 (REA796),  $\alpha$ CD11c-VioBlue (REA754) and  $\alpha$ CD11b-VioGreen (REA592) from Miltenyi Biotec (Bergisch Gladbach, Germany),  $\alpha$ CD19-FITC (1D3) and  $\alpha$ Ly6G-FITC (1A8) from BD Bioscience (Heidelberg, Germany),  $\alpha$ CD86-PE (GL-1) and  $\alpha$ CD64-PerCP-Cy5.5 (X54-5/7.1) from BioLegend (Santa Clara, CA, USA) and  $\alpha$ CD103-APC (2E7) and  $\alpha$ F4/80-APC (BM8) from eBioscience (Santa Clara, CA, USA). The gating strategy for DC subsets was modified from Boriello et al.<sup>61</sup> and Cerovic et al.<sup>48</sup>

Viable cells were identified by the Fixable Viability Stain 780 (BD Bioscience, Heidelberg, Germany). Data were acquired by BD FACSCanto II and analyzed by FlowJo v.10 (BD Bioscience, Heidelberg, Germany).

### RNA isolation and quantitative real-time PCR

For gene expression analysis, BMDCs were stimulated for 4 h, unless otherwise stated, with 200 nM BPI, 10 nM bLP, 10 ng/mL LPS and 5  $\mu$ g/mL Zymd. Cell lysis and RNA isolation was performed using RNeasy Mini Kit (QIAGEN, Hilden, Germany). For lysate homogenization and DNA digestion QIAshredder homogenizer columns (QIAGEN, Hilden, Germany) and TURBO DNA-free Kit (Thermo Fisher Scientific, Waltham, MA, USA) were applied. cDNA was synthesized with iScript Advanced cDNA Synthesis Kit (Bio-Rad Laboratories, Feldkirchen, Germany). Quantitative real-time PCR was performed in triplicates with LightCycler 480 SYBR Green I Master (Roche, Basel, Switzerland) for *Hprt* (fwd: 5'-GTT GGA TAC AGG CCA GAC TTT GTT G-3', rev: 5'-GAT TCA ACT TGC GCT CAT CTT AGG C-3'), *Ifng* (fwd: 5'-AGC GGC TGA CTG AAC TCA GAT TGT AG-3', rev: 5'-GTC ACA GTT TTC AGC TGT ATA GGG-3'), *Il2* (fwd: 5'-GAG CAG GAT GGA GAA TTA CAG G-3', rev: 5'-TCC AGA ACA TGC CGC AGA-3'), *Il6* (fwd: 5'-AAC CAC GGC CTT CCC TAC TTC-3', rev: 5'-GCC ATT GCA CAA CTC TTT TCT CAT-3'), *Il12a* (fwd: 5'-GGC CAC CCT TGC CCT CCT A-3', rev: 5'-GGG CAG GCA GCT CCC TCT T-3'), *Il12b* (fwd: 5'-TCC AGC GCA AGA AAG AAA AGA TG-3', rev: 5'-AAA AGC CAA CCA AGC AGA AGA CAG-3'), *Il17a* (fwd: 5'-ATC AGG ACG CGC AAA CAT GA-3', rev: 5'-TTG GAC ACG CTG AGC TTT GA-3'), *Il22* (fwd: 5'-CGC TGC CCG TCA ACA CCC GG-3', rev: 5'-CTG ATC CTT AGC ACT GAC TCC TCG-3'), *Il23a* (fwd: 5'-ATG CTG GAT TGC AGA GCA GTA-3', rev: 5'-GCT CCC CTT TGA AGA TGT CAG-3') and *Tnf* (fwd: 5'-ATG AGC ACA GAA AGC ATG ATC-3', rev: 5'-TAC AGG CTT GTC ACT CGA ATT-3') with intron flanking primers to ensure mRNA specific amplification purchased from Biomers (Ulm, Germany), Thermo Fisher Scientific (Waltham, MA, USA) or Microsynth Seqlab (Göttingen, Germany). PCR reaction was performed using ABI PRISM 7900HT Sequence Detection System (Thermo Fisher Scientific, Waltham, MA, USA) and LightCycler 480II (Roche, Basel, Switzerland). SDS software version 2.4 (Thermo Fisher Scientific, Waltham, MA, USA) was used to analyze the gene expression. Data were normalized to *Hprt* and calculated either by the  $\Delta\Delta$ CT method as fold induction compared to the NT control<sup>62</sup> or by using a standard curve.

### Gene chip microarray assay

BMDCs were stimulated with 200 nM hu and muBPI for 4 h before stabilization in RLT buffer (QIAGEN, Hilden, Germany). Sample processing, microarray hybridization (Affymetrix Mouse Gene 2.0 ST arrays) and measurements was carried out as described in the Affymetrix GeneChip WT PLUS Reagent Kit User Manual (Affymetrix, Santa Clara, CA, USA) by an Affymetrix Service Provider (KFB, Regensburg, Germany).

### Confocal imaging

BMDCs were seeded on  $\mu$ -Slide VI 0.5 Glass Bottom (ibidi, Martinsried, Germany) and stimulated for 2 h at 37°C with 200 nM BPI labeled with NT647 (Alexa 647) in PBS pH 7.4 (Monolith NT Protein Labeling Kit RED-NHS, NanoTemper Technologies, Munich, Germany). Cells were fixed with 4% methanol-free formaldehyde (Thermo Fisher Scientific, Waltham, MA, USA) and mounted with mounting medium containing DAPI (ibidi, Martinsried, Germany). ActinGreen (Thermo Fisher Scientific, Waltham, MA, USA) was used for actin staining. Imaging was performed using a Leica TCS SP5 confocal laser microscope and the Leica Application Suite, version 2.7.3.9723 (Leica, Wetzlar, Germany).

### Immunoblot analysis

For immunoblotting BMDCs were seeded on day 6 and were allowed to finally differentiate overnight. Cells were stimulated for 1 h with 100 nM, 200 nM and 400 nM BPI and lysed by 1-fold SDS sample buffer (62.5 mM Tris-HCl pH 6.8, 2% SDS, 10% glycerol and a mixture of cOmplete and PhosSTOP; Roche, Basel, Switzerland) followed by sonification and heating. Samples were mixed with 5-fold sample buffer (0.312 mM Tris-HCl pH 6.8, 10% SDS, 50% glycerol, 0.05% Bromophenol blue and 0.25 mM DTT) and resolved by SDS-PAGE. Proteins were blotted onto a nitrocellulose membrane using the Trans-Blot TurboTM Transfer System (Bio-Rad Laboratories, Feldkirchen, Germany) followed by blocking with 5% milk powder. Antibodies targeting p-Jnk (Thr183 and Tyr185, 81E11), Jnk2 (56G8), p-p38 (Thr180 and Tyr182, polyclonal), p38 (polyclonal), p-Erk1/2 (Thr202 and Tyr204, 197G2) and Erk1/2 (polyclonal) produced in rabbit were obtained from Cell Signaling Technologies (Frankfurt am Main, Germany). Mouse anti- $\beta$ -Actin (AC-15) was from Sigma Aldrich (Taufkirchen, Germany). Horseradish peroxidase coupled antibodies rabbit- $\alpha$ -murine (polyclonal) and donkey- $\alpha$ -rabbit (polyclonal) were purchased from Dianova (Hamburg, Germany) and were used for protein visualization by enhanced chemiluminescence. ChemoStar Imager and software (Intas Science Imaging Instruments, Göttingen, Germany) were used for imaging.

### Microbiota analysis

Nucleic acids were extracted from  $\sim$ 50 mg cecal contents of co-housed mice applying repeated bead-beating protocol. Extraction of nucleic acids, real-time PCR quantification of bacterial 16S rRNA gene copy numbers and 16S microbiome sequencing of V1/V3 variable regions were performed as described in detail before.<sup>63</sup> Except automated isothermal amplification, chip loading and high-throughput sequencing was carried out using the IonChef instrument and an IonTorrent Genestudio S5 Plus sequencer (Thermo Fisher Scientific, Waltham, MA, USA). Raw sequencing reads were subjected to Trimmomatic 0.39 for sliding window trimming applying a windows size of 25 and a quality cutoff of 20. Cutadapt 3.4 was used for demultiplexing and removal of sequencing adapters and 16S PCR primers.<sup>64</sup> Amplicon sequence variants (ASV) were generated from demultiplexed reads (31,231  $\pm$  2,432) using a dada2-based Bioconductor workflow together with the the All-Species Living Tree Project (LTP) reference database release 12\_2020 was used for taxonomic classification of ASVs.<sup>65,66</sup> Alpha- and beta-diversity analyses were conducted applying the phyloseq package version 1.36. Species Richness was represented by summarized ASVs. Principal coordinates were calculated from

unweighted UniFrac distances. Significant differentially abundant taxa were determined with DESeq2 after computing geometric means for each ASV across all samples.

Significance of principal components analysis cluster differences were tested by a non-parametric multilevel pairwise Permutational Multivariate Analysis of Variance (PERMANOVA). p-values were adjusted using the Benjamini-Hochberg method.

### QUANTIFICATION AND STATISTICAL ANALYSIS

GraphPad Prism, version 7 (GraphPad Software, San Diego, CA, USA) was used for statistical analysis and depiction. Results are shown as mean  $\pm$  standard error of the mean (SEM). p-values  $<0.05$  were considered statically significant. Number of biological replicates are indicated as n. In all *in vitro* or *ex vivo* experiments using BMDCs, BMDMs, PLCs, cDCs or cells derived from lymph nodes or spleens, a biological replicate is defined as an experiment performed in cells derived from an individual mouse. In all *in vivo* experiments, a biological replicate is defined as an experiment performed using an individual animal or materials thereof. Statistic tests were used as indicated. All test used were two-sided and performed on measurements from distinct samples as depicted in the figures.

**Cell Reports, Volume 43**

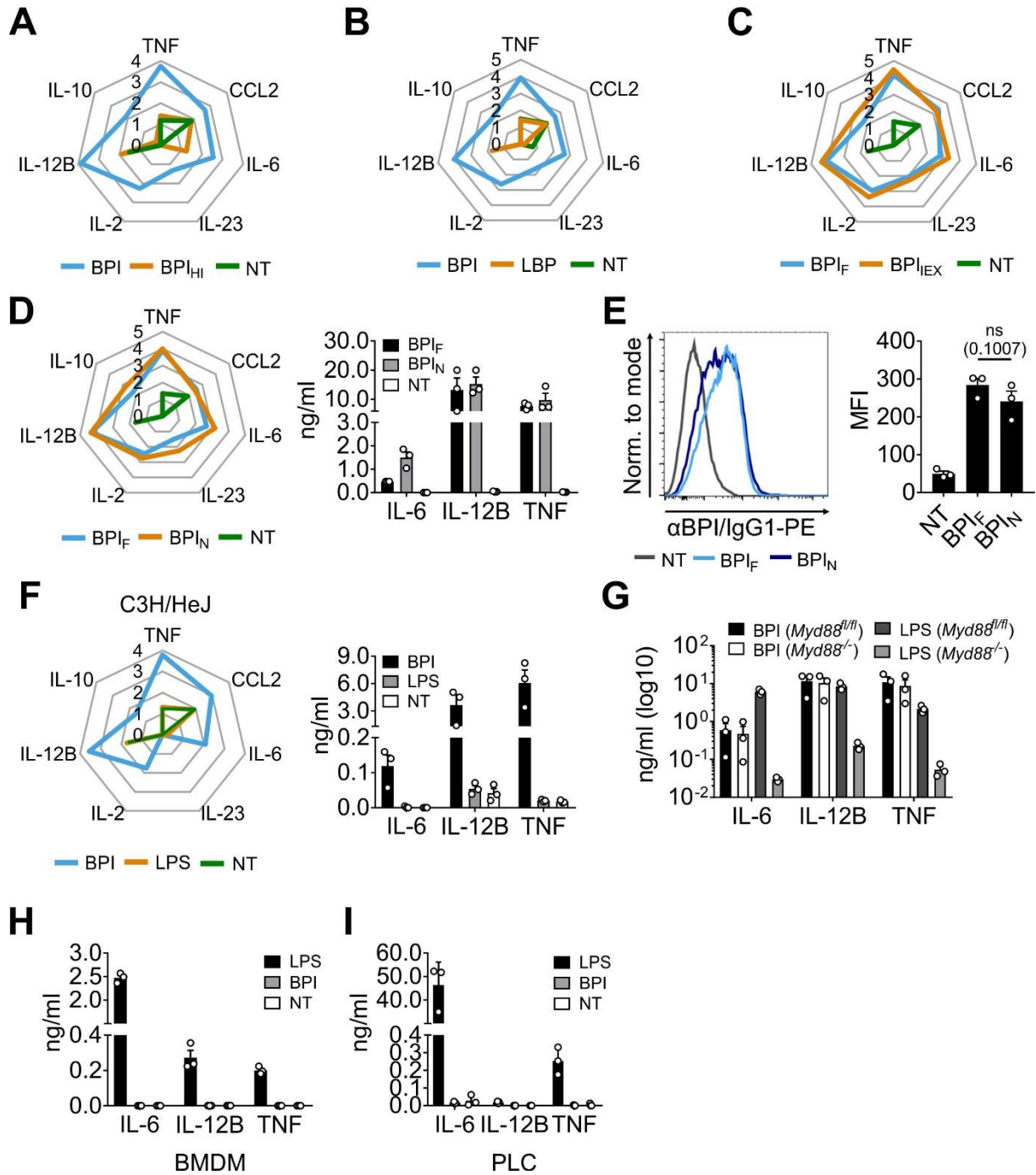
**Supplemental information**

**Bactericidal/permeability-increasing**

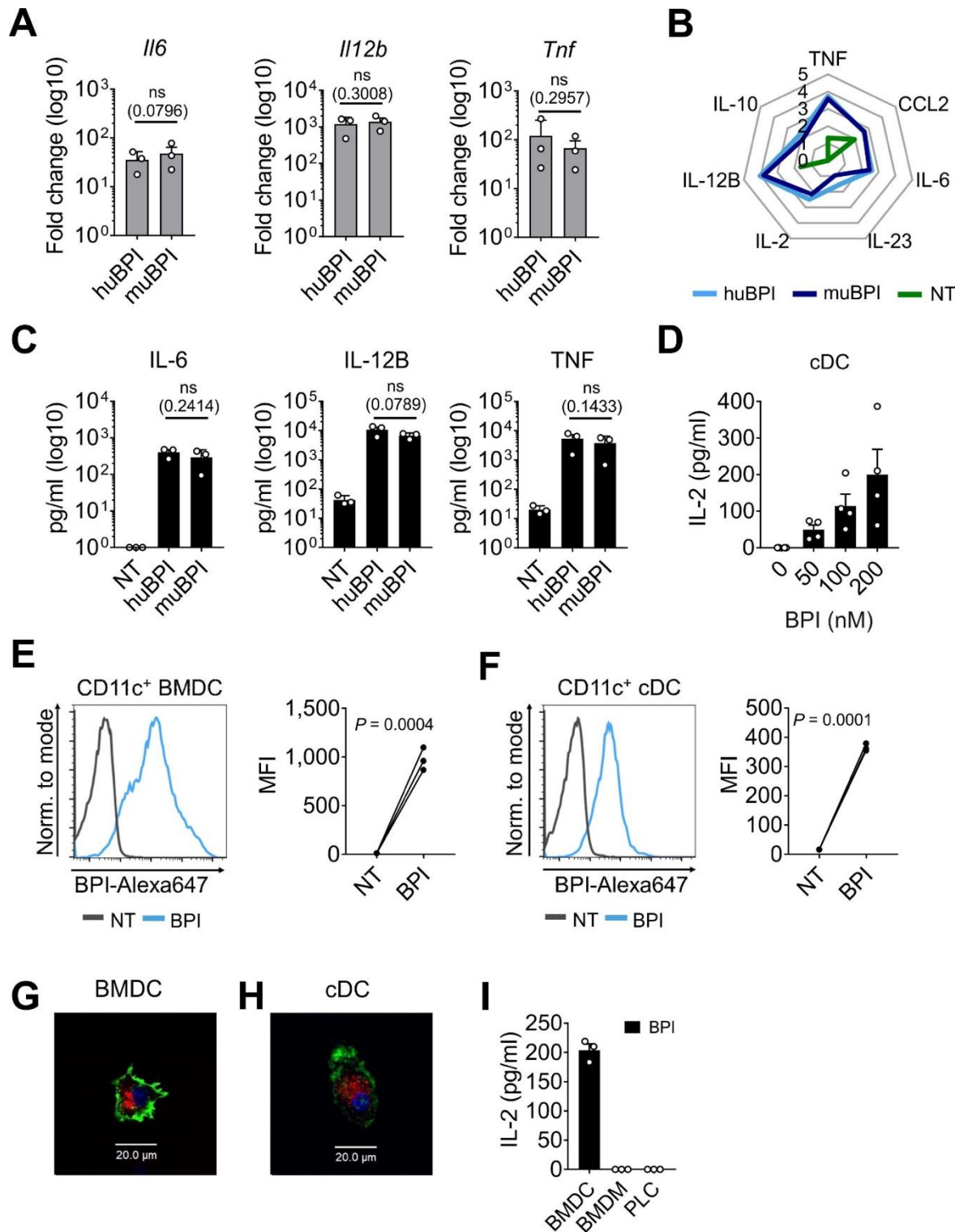
**protein instructs dendritic cells**

**to elicit Th22 cell response**

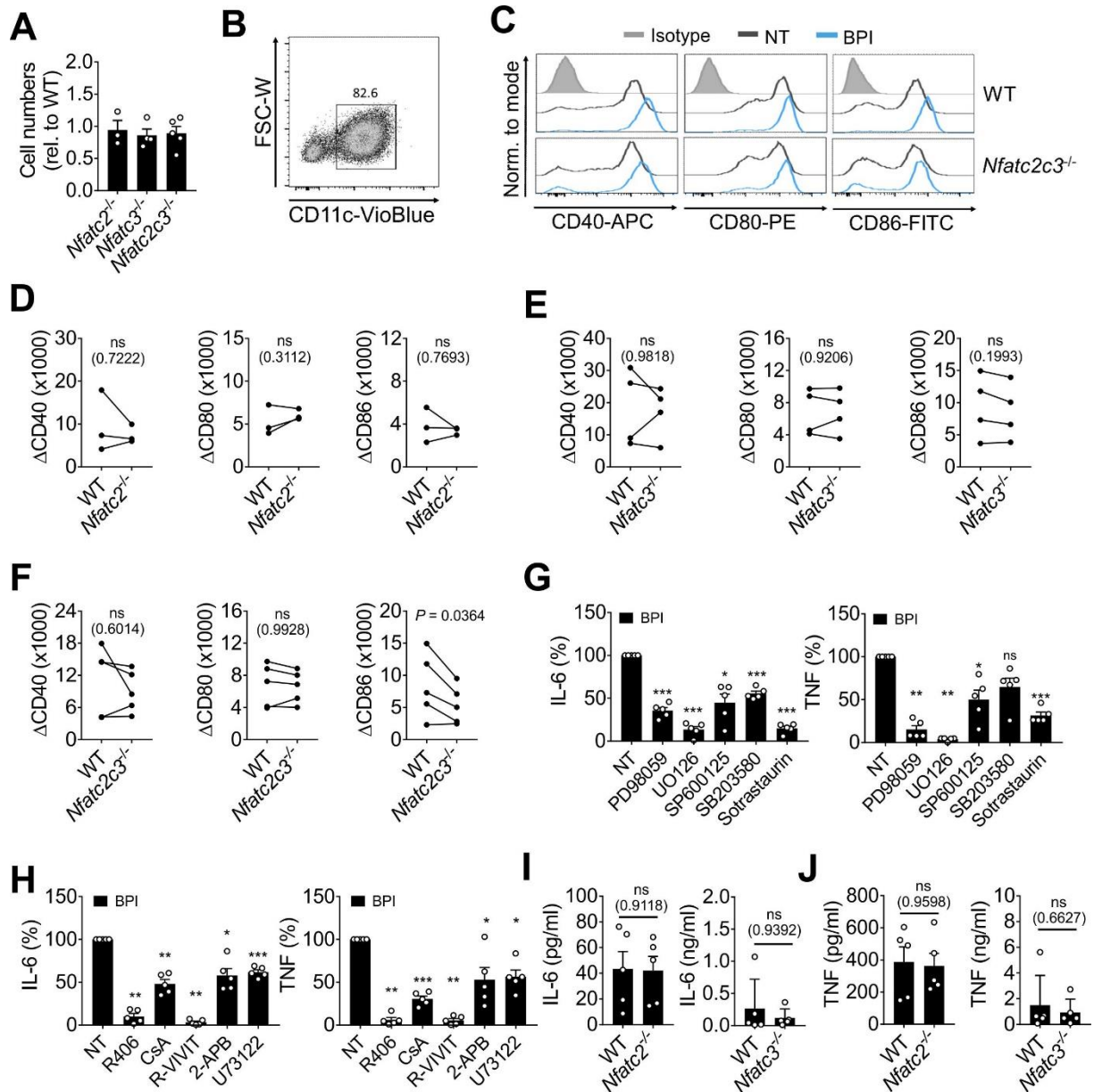
**Sigrid Bülow, Katharina U. Ederer, Jonas M. Holzinger, Lisa Zeller, Maren Werner, Martina Toelge, Christina Pfab, Sarah Hirsch, Franziska Göpferich, Andreas Hiergeist, Friederike Berberich-Siebelt, and André Gessner**



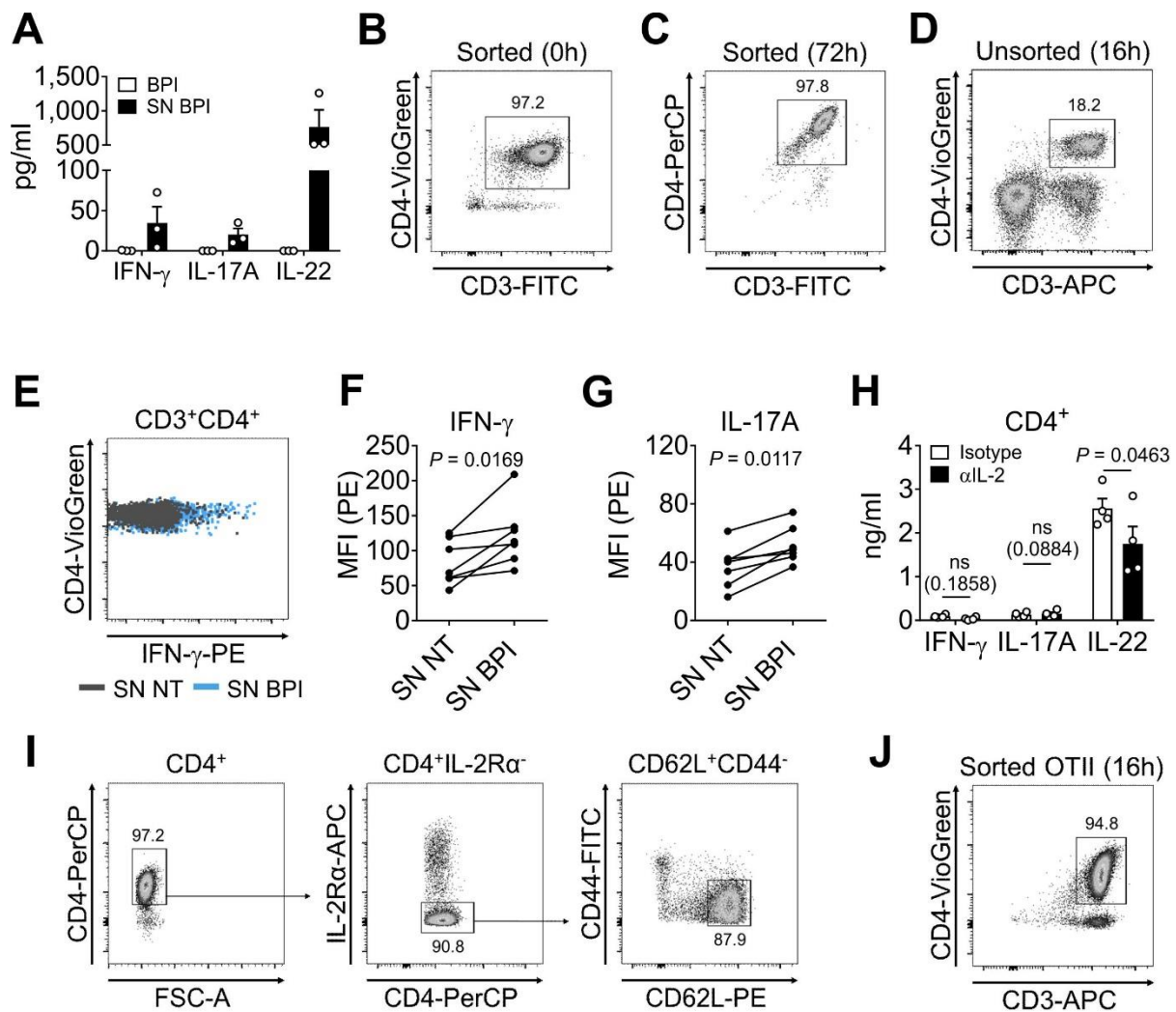
**Supplementary Figure 1. Purity controls of recombinant BPI.** (A-D) TNF, CCL2, IL-2, IL-6, IL-10, IL-12B and IL-23 secretion by BMDCs after stimulation with heat-inactivated BPI (BPI<sub>HI</sub>; A), LBP (B), BPI purified on an ion-exchange column with size-exclusion (BPI<sub>IEX</sub>; C) and neutrophil-derived BPI (BPI<sub>N</sub>;D) compared to stimulation with BPI purified on an  $\alpha$ Flag column (BPI<sub>F</sub>) and untreated cells (NT; n = 3). (E) Representative histogram and summarized data of flow cytometric analysis of the association of BPI<sub>F</sub> and BPI<sub>N</sub> to CD11c<sup>+</sup> gated BMDCs (n = 3). (F) Cytokine induction after stimulation with BPI and LPS by BMDCs derived from C3H/HeJ mice (n = 3). (G) IL-6, IL-12B and TNF secretion compared between *Myd88*<sup>fl/fl</sup> and *Myd88*<sup>-/-</sup> BMDCs after stimulation with BPI and LPS (n = 3). (H, I) IL-6, IL-12B and TNF secretion in BMDMs (H) and PLCs (I) upon stimulation with LPS and BPI. Cytokine levels in spider diagrams are presented as pg/ml in a logarithmic scale (A-D, F). Results are shown as means  $\pm$  SEM (D-I). Student's ratio paired *t*-test was applied for statistical testing. Related to Figure 1.



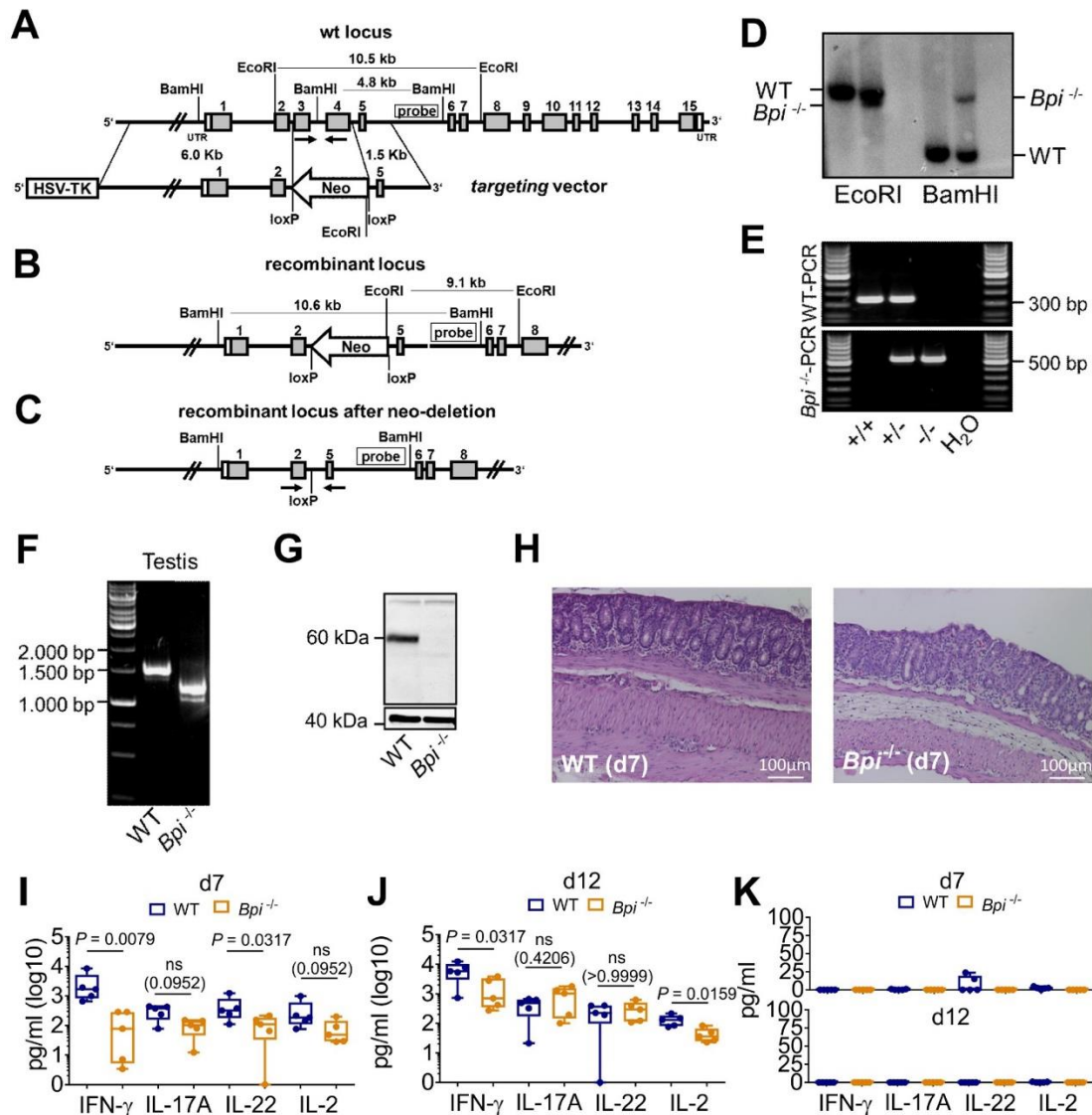
**Supplementary Figure 2. Activation of BMDCs by BPI.** (A) Gene expression of *Il6*, *Il12b* and *Tnf* after stimulation with huBPI and muBPI ( $n = 3$ ). (B, C) Cytokine levels induced by huBPI and muBPI compared to untreated cells ( $n = 3$ ). (D) IL-2 secretion in cDCs upon stimulation with BPI. (E, F) Representative histograms and summarized data of flow cytometric analysis showing association of Alexa647-labeled BPI with BMDCs and cDCs (E, F;  $n = 3$ ). (G, H) Confocal microscopy of BMDCs (G) and cDCs (H) incubated with Alexa647-labeled BPI for 2 h (BPI: red, DAPI: blue, Actin: green). (I) IL-2 secretion in BMDCs, BMDMs and PLCs upon stimulation with BPI. Cytokine levels in the spider diagram are presented as pg/ml in a logarithmic scale. Results in bar charts are shown as means  $\pm$  SEM (A, C, D, I). Student's ratio paired  $t$ -test was applied for statistical testing. Related to Figure 2.



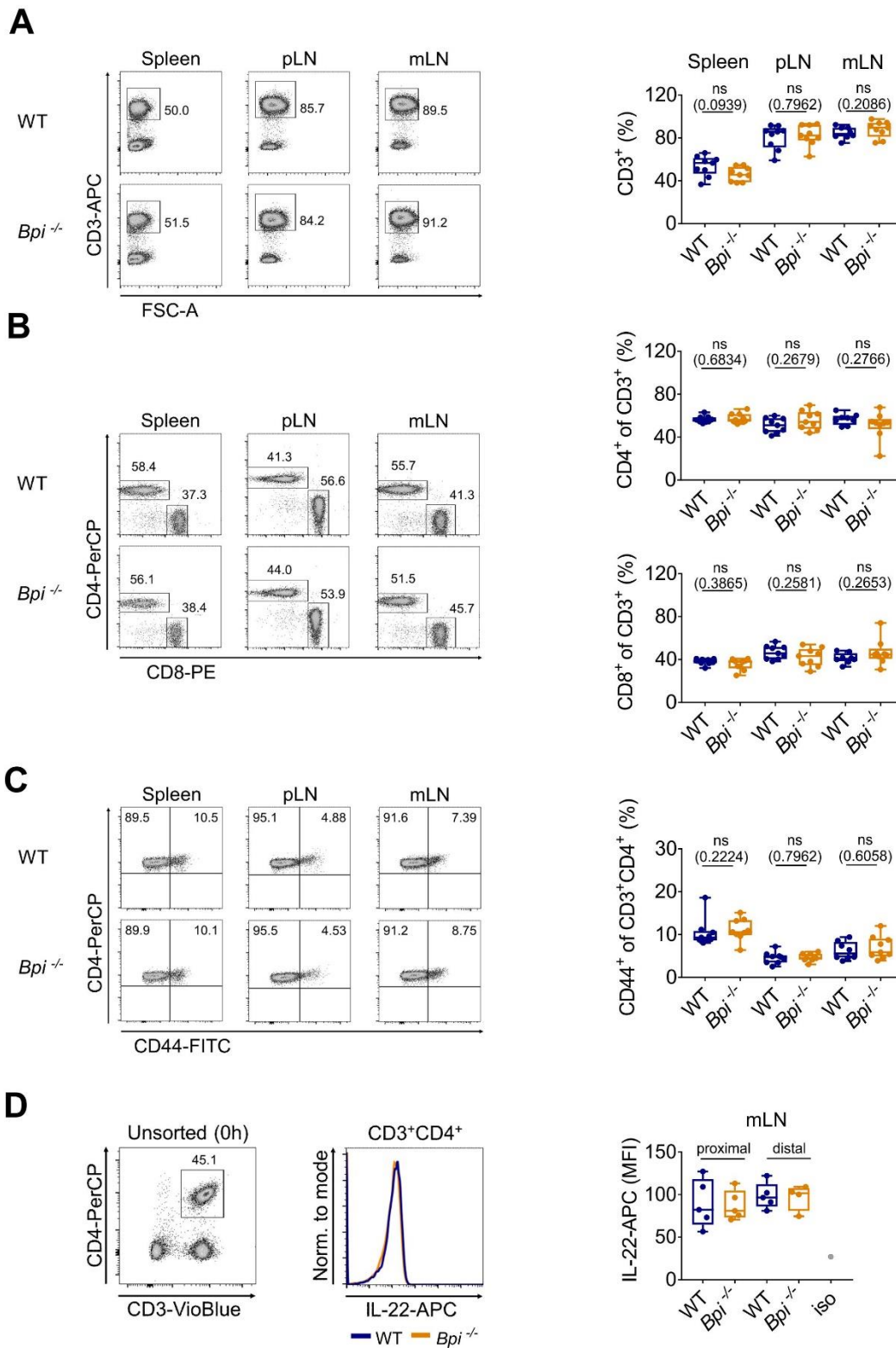
**Supplementary Figure 3. Signaling pathways induced by BPI in BMDCs.** (A) Cell yield from cultured *Nfatc2*<sup>-/-</sup> (n = 3), *Nfatc3*<sup>-/-</sup> (n = 4), and *Nfatc2c3*<sup>-/-</sup> (n = 5) BMDCs shown in relation to corresponding WT mice. (B) Representative dot plot showing flow cytometric gating of CD11c<sup>+</sup> BMDCs for cell surface marker analysis of *Nfat* deficient mice. (C) Representative histograms for CD40, CD80 and CD86 surface expression for untreated or BPI-stimulated *Nfatc2c3*<sup>-/-</sup> and WT mice as measured by flow cytometry. (D-F) Summarized data of flow cytometric analysis showing CD40, CD80 and CD86 surface expression after BPI stimulation of *Nfatc2*<sup>-/-</sup> (D; n = 3), *Nfatc3*<sup>-/-</sup> (E; n = 4) and *Nfatc2c3*<sup>-/-</sup> (F; n = 5) BMDCs and corresponding WT CD11c<sup>+</sup> BMDCs. Median-fluorescence intensities (MFIs) from untreated cells were subtracted from MFIs of BPI-stimulated cells ( $\Delta$ CD40,  $\Delta$ CD80,  $\Delta$ CD86). (G, H) Inhibition of BPI induced IL-6 and TNF secretion by PD98059, UO126, SP600125, SB203580 and Sotrastaurin (G) as well as R406, Cyclosporin A (CsA), 11R-VIVIT, 2-APB and U73122 (H) compared to untreated cells (NT; n = 5). (I, J) IL-6 (I) and TNF (J) concentrations for BPI-stimulated *Nfatc2*<sup>-/-</sup> and *Nfatc3*<sup>-/-</sup> BMDCs compared to corresponding WT cells (BPI 100 nM; n = 5). Data are shown as means  $\pm$  SEM (A, G-J). Statistical testing was performed using Student's ratio paired *t*-test with \* *P* < 0.05, \*\* *P* < 0.01, \*\*\* *P* < 0.001, \*\*\*\* *P* < 0.0001. Related to Figure 3.



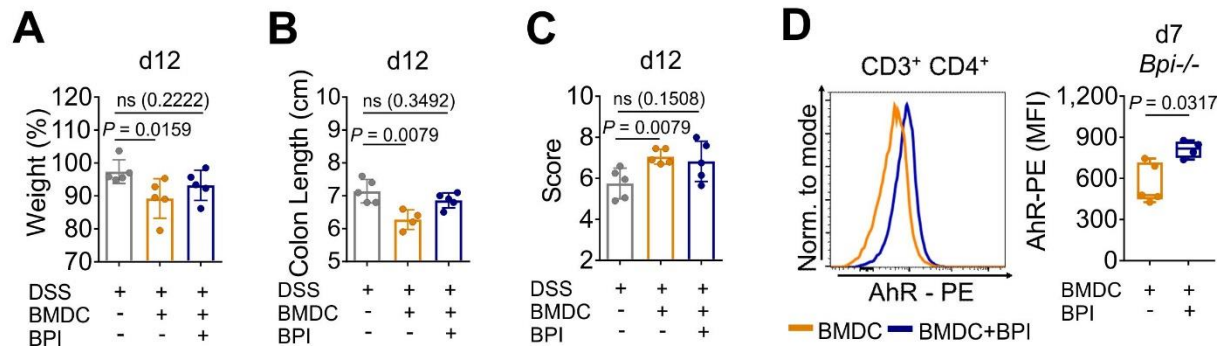
**Supplementary Figure 4. BPI-dependent CD4<sup>+</sup> T-cell activation and differentiation.** (A) IFN- $\gamma$ , IL-17A and IL-22 levels in the supernatants of unsorted spleen cells and pLNC stimulated with either BPI or SN BPI for 24 h ( $n = 3$ ). (B-D) Representative dot blots for purity control (B) and gating of CD3<sup>+</sup>CD4<sup>+</sup> cells (C, D) as measured by flow cytometry. (E-G) Secretion assay for IFN- $\gamma$  (E, F) and IL-17A (G) in CD3<sup>+</sup>CD4<sup>+</sup> cells after activation of pooled splenic and pLN cells with SN BPI for 16 h ( $n = 7$ ). Representative dot blot for IFN- $\gamma$  (E). (H) IFN- $\gamma$ , IL-17A and IL-22 levels in the supernatants of CD4<sup>+</sup> pLN cells after 24 h stimulation with SN BPI preincubated with an  $\alpha$ IL-2 antibody for 1 h ( $n = 4$ ). (I) Fluorescence-activated cell sorting of naive CD4<sup>+</sup> T cells characterized by a CD4<sup>+</sup>IL-2R $\alpha$ <sup>-</sup>CD44<sup>-</sup>CD62L<sup>+</sup> phenotype. (J) Representative dot blot for gating of OTII CD3<sup>+</sup>CD4<sup>+</sup> cells. Cells were activated in the presence of  $\alpha$ CD3 and  $\alpha$ CD28 antibodies (A, C-H). Magnetic-activated cell sorting was performed in (B-D, J). Data are shown as means  $\pm$  SEM (A, H). Statistical testing was performed using Student's ratio paired  $t$ -test. Related to Figure 4 and 5.



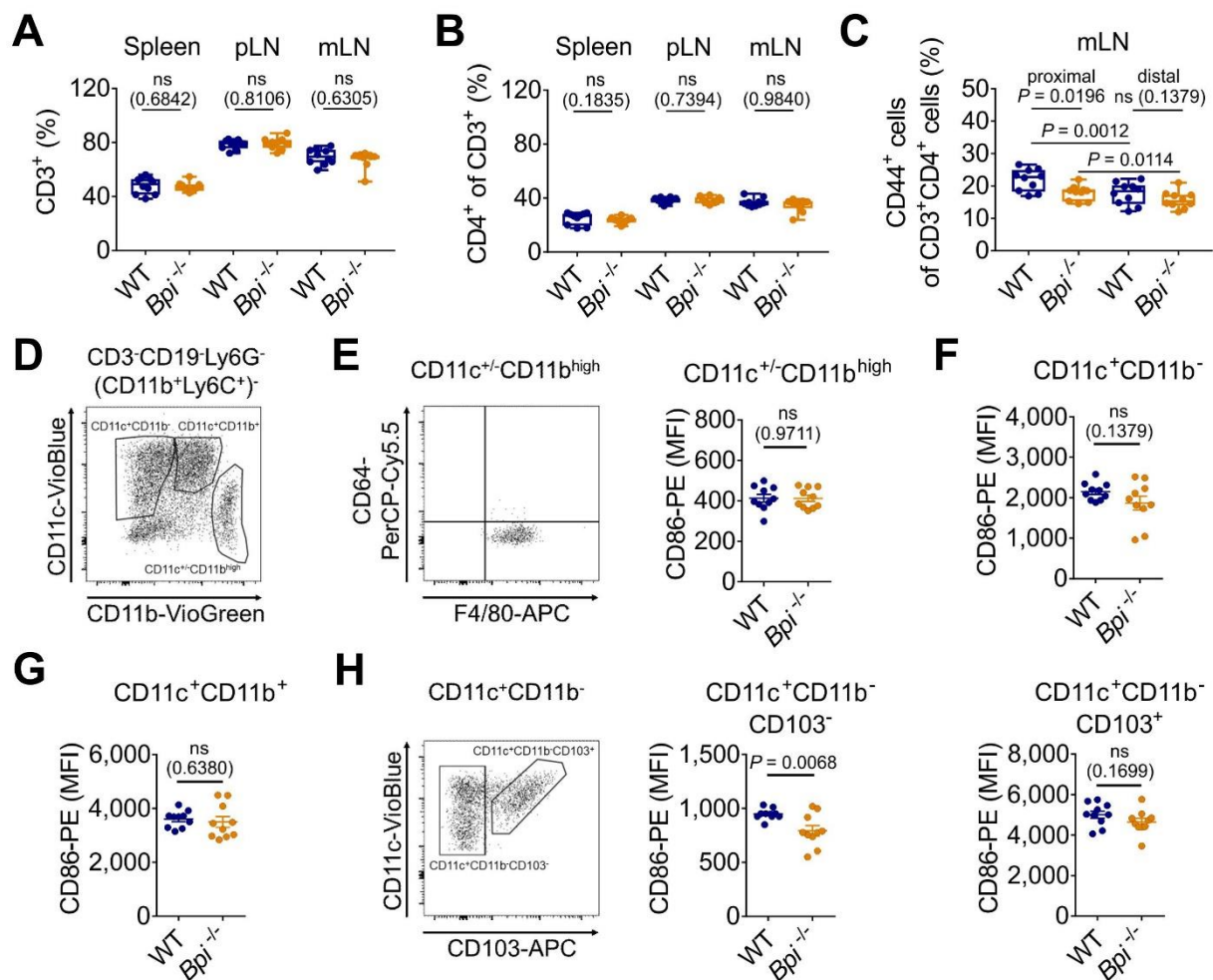
**Supplementary Figure 5. Generation of *Bpi*<sup>-/-</sup> mice and phenotype in a DSS-induced colitis model. (A)** Gene targeting strategy for the generation of *Bpi*<sup>-/-</sup> mice. Grey boxes represent the numbered exons of the *Bpi* wild-type locus, white boxes untranslated regions (UTR). The target of the radioactive probe and restriction sites for BamHI and EcoRI and sizes for the expected fragments are indicated. The neomycin resistance cassette (Neo) of the targeting vector is flanked by a 6.0 kb and 1.5 kb arm. Additionally, the targeting vector encodes for a herpes simplex virus (HSV) thymidine kinase (HSV-TK). **(B)** Representation of the recombinant locus after successful homologous recombination. **(C)** The mature locus after excision of the neomycin resistance by Cre-mediated recombination. **(D)** Southern blot analysis of DNA isolated from wildtype (WT)-embryonic stem cells (ESC) and BPI-deficient (*Bpi*<sup>-/-</sup>) recombinant-ESC. Expected sizes for amplified WT and *Bpi*<sup>-/-</sup> fragments are indicated. **(E)** PCR genotyping for biopsies of WT (+/+), heterozygous (+/-) or *Bpi*<sup>-/-</sup> (-/-) mice. **(F)** RT-PCR analysis of RNA from testis of WT and *Bpi*<sup>-/-</sup> mice. **(G)** Expression of BPI in testis tissue lysates of WT and *Bpi*<sup>-/-</sup> mice analyzed by western blot analysis (n = 3). **(H-K)** Analysis of C57BL/6J WT and *Bpi*<sup>-/-</sup> mice on d7 and d12 after exposure to 1.8% DSS-containing water for seven days and a regeneration phase of five days. **(H)** Representative histological cross-sections of the distal colon on d7 (HE stain). **(I, J)** IFN-γ, IL-17A, IL-22 and IL-2 levels in the supernatants of mLNC harvested on d7 and activated by αCD3 and αCD28 antibodies for 24 h (d7, n = 5; I) and for 48 h (d12, n = 5; J). **(K)** Corresponding IFN-γ, IL-17A, IL-22 and IL-2 levels in the supernatants of mLNC harvested on d7 and d12 without αCD3 and αCD28 antibodies (n = 5). Data are depicted as box plots showing median, upper and lower quartiles and whiskers indicating minimal and maximal values (I-K). Statistical testing was performed using two-tailed Mann-Whitney-U-test. Related to Figure 6.



**Supplementary Figure 6. T-cell immunophenotyping of co-housed C57BL/6J WT and *Bpi*<sup>-/-</sup> mice in SPF housing.** (A-C) T-cell immunophenotyping of co-housed C57BL/6J and *Bpi*<sup>-/-</sup> mice (n = 9). Representative dot plots for flow cytometric analysis of expression of CD3 on all cells (A), CD4 and CD8 on CD3<sup>+</sup> cells (B) and CD44 on CD3<sup>+</sup>CD4<sup>+</sup> cells (C). Cells in the indicated gates as a percentage of the respective parent cell population are indicated. (D) Gating strategy, representative histogram and MFI for IL-22 in CD3<sup>+</sup>CD4<sup>+</sup> proximal and distal mLN cells of WT and *Bpi*<sup>-/-</sup> mice. Data are depicted as box plots showing median, upper and lower quartiles and whiskers indicating minimal and maximal values. Statistical testing was performed using two-tailed Mann-Whitney-U-test. Related to Figure 6.



**Supplementary Figure 7. Influence of BPI-stimulated BMDCs on DSS-induced colitis (A-D)** Analysis of *Bpi*<sup>-/-</sup> mice either without transfer or transferred with BMDCs ± BPI on day one of exposure to 1.8% (A-C) or 2.5% (D) DSS-containing water for seven days (A-D) and a regeneration phase of five days (A-C). Relative body weight (A), colon length (B) and histological score (C) on d12 (n = 5). **(D)** Representative histogram and MFI of flow cytometric analysis showing intracellular AhR expression in CD3<sup>+</sup>CD4<sup>+</sup> cells derived from mLN of mice transferred with BMDCs ± BPI (d7; n = 5 and n = 4, respectively). Data are depicted as box plots showing median, upper and lower quartiles and whiskers indicating minimal and maximal values (D) or means ± SEM (A-C). Statistical testing was performed using two-tailed Mann-Whitney-U-test. Related to Figure 6.



**Supplementary Figure 8. T-cell and DC immunophenotyping of C57BL/6J WT and *Bpi*<sup>-/-</sup> mice co-housed in a conventional animal facility (n = 10).** (A-C) Flow cytometric analysis of the percentage of CD3<sup>+</sup> cells in spleen and lymph nodes (A), CD4<sup>+</sup> in CD3<sup>+</sup> cells as well as (B), CD44<sup>+</sup> in CD3<sup>+</sup>CD4<sup>+</sup> cells (C) as shown for spleen cells, pLNCs and mLNCs. (D-H) Flow cytometric immunophenotyping of DCs and macrophages derived from proximal mesenteric lymph nodes. Strategy to analyze DC and macrophage populations by gating for CD3<sup>-</sup>CD19<sup>-</sup>Ly6G<sup>-</sup> cells with exclusion of CD11b<sup>+</sup>Ly6C<sup>+</sup> double-positive subsets (D). Expression of CD86 in CD11c<sup>+</sup>CD11b<sup>high</sup> (E) CD11c<sup>+</sup>CD11b<sup>-</sup> (F) CD11c<sup>+</sup>CD11b<sup>+</sup> (G) as well as CD11c<sup>+</sup>CD11b<sup>-</sup>CD103<sup>-</sup> and CD11c<sup>+</sup>CD11b<sup>-</sup>CD103<sup>+</sup> cells (H). Data are depicted as box plots showing median, upper and lower quartiles and whiskers indicating minimal and maximal values (A-C) or as mean ± SEM (E-H). Statistical testing was performed using two-tailed Mann-Whitney-U-test (A-C) or unpaired Student's *t*-test (D-H). Related to Figure 7.

**Supplementary Table 1. Primer pairs used in this study.** Related to key resources table, STAR★Methods.

Primer Sequence	Source	Identifier
<i>Hprt</i> fwd 5'-GTT GGA TAC AGG CCA GAC TTT GTT G-3'	Biomers	N/A
<i>Hprt</i> rev 5'-GAT TCA ACT TGC GCT CAT CTT AGG C-3'	Biomers	N/A
<i>Ifng</i> fwd 5'-AGC GGC TGA CTG AAC TCA GAT TGT AG-3'	Thermo Fisher	N/A
<i>Ifng</i> rev 5'-GTC ACA GTT TTC AGC TGT ATA GGG-3'	Thermo Fisher	N/A
<i>Il12a</i> fwd 5'-GGC CAC CCT TGC CCT CCT A-3'	Biomers	N/A
<i>Il12a</i> rev 5'-GGG CAG GCA GCT CCC TCT T-3'	Biomers	N/A
<i>Il12b</i> fwd 5'-TCC AGC GCA AGA AAG AAA AGA TG-3'	Thermo Fisher	N/A
<i>Il12b</i> rev 5'-AAA AGC CAA CCA AGC AGA AGA CAG-3'	Thermo Fisher	N/A
<i>Il17a</i> fwd 5'-ATC AGG ACG CGC AAA CAT GA-3'	Biomers	N/A
<i>Il17a</i> rev 5'-TTG GAC ACG CTG AGC TTT GA-3'	Biomers	N/A
<i>Il2</i> fwd 5'-GAG CAG GAT GGA GAA TTA CAG G-3'	Microsynth	N/A
<i>Il2</i> rev 5'-TCC AGA ACA TGC CGC AGA-3'	Microsynth	N/A
<i>Il22</i> fwd 5'-CGC TGC CCG TCA ACA CCC GG-3'	Biomers	N/A
<i>Il22</i> rev 5'-CTG ATC CTT AGC ACT GAC TCC TCG-3'	Biomers	N/A
<i>Il23a</i> fwd 5'-ATG CTG GAT TGC AGA GCA GTA-3'	Thermo Fisher	N/A
<i>Il23a</i> rev 5'-GCT CCC CTT TGA AGA TGT CAG-3'	Thermo Fisher	N/A
<i>Il6</i> fwd 5'-AAC CAC GGC CTT CCC TAC TTC-3'	Thermo Fisher	N/A
<i>Il6</i> rev 5'-GCC ATT GCA CAA CTC TTT TCT CAT-3'	Thermo Fisher	N/A
<i>Tnf</i> fwd 5'-ATG AGC ACA GAA AGC ATG ATC-3'	Thermo Fisher	N/A
<i>Tnf</i> rev 5'-TAC AGG CTT GTC ACT CGA ATT-3'	Thermo Fisher	N/A